Distribution Agreement

In presenting this thesis or dissertation as a partial fulfillment of the requirements for an advanced degree from Emory University, I hereby grant to Emory University and its agents the non-exclusive license to archive, make accessible, and display my thesis or dissertation in whole or in part in all forms of media, now or hereafter known, including display on the world wide web. I understand that I may select some access restrictions as part of the online submission of this thesis or dissertation. I retain all ownership rights to the copyright of the thesis or dissertation. I also retain the right to use in future works (such as articles or books) all or part of this thesis or dissertation.

Signature:

_____ _____

Jack Trieu Date

Ring Chain Isomerism: Ligands for Mediating Two-Electron Reactivity with First-Row Transition Metals

By

Jack Trieu
Master of Science

Chemistry

_____

Christopher Scarborough
Advisor

_____

Simon Blakey
Committee Member

_____

Frank McDonald
Committee Member

Accepted:

_____

Lisa A. Tedesco, Ph.D.
Dean of the James T. Laney School of Graduate Studies

_____

Date

Ring Chain Isomerism: Ligands for Mediating Two-Electron Reactivity with First-Row Transition Metals

By

Jack Trieu
B.A., Hamilton College, 2011

Advisor: Christopher Scarborough, Ph.D.

An abstract of a thesis submitted to the Faculty of the
James T. Laney School of Graduate Studies of Emory University
in partial fulfillment of the requirements for the degree of
Master of Science
in Chemistry
2014

Abstract

Ring Chain Isomerism: Ligands for Mediating Two-Electron Reactivity with First-Row Transition Metals

By Jack Trieu

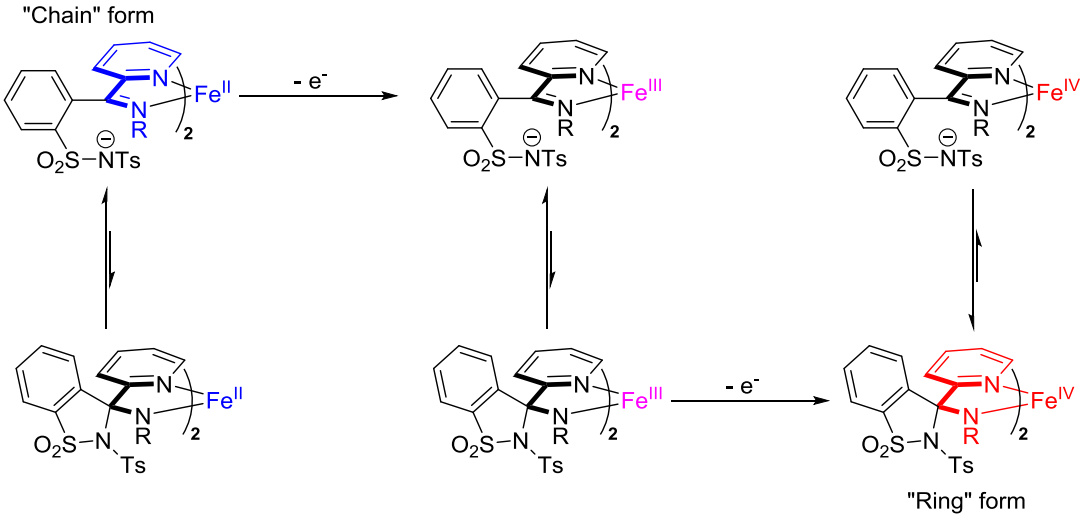

The goal of this project is to generate ligands that can induce two-electron reactivity in first-row transition metals for catalysis. The primary focus of this research is to develop ligands capable of facilitating two-electron reactivity with first-row transition metals. These ligands, termed “electronically responsive ligands” (ERLs), are designed to undergo ring chain tautomerism (RCT) to stabilize $Fe^{II/IV}$ cycles and disfavor $Fe^{II/III}$ cycles. The core functionality in the approach to RCT in these ligands is to utilize an imino-pyridine and a pendant anionic nitrogen donor, specifically a sulfonimidate. The imino-pyridine will allow for stabilization of an Fe^{II} center; interconversion to the amido-pyridine, through intramolecular nucleophilic attack by the sulfonimidate, affects the stabilization of Fe^{IV}. Initially, the synthesis towards ERLs proved difficult due to the presence of multiple reactive sites in sulfonimides. Key intermediates obtained in the synthesis of the target ERLs exhibited the desired RCT in the absence of a coordinating metal. Unfortunately, the synthesis of these key intermediates was low-yielding. Furthermore, it was observed that sterics can bias RCT selectivity, with increased steric bulk disfavoring the ring form over the chain form. Taken together, these observations of ring chain tautomerism from our key intermediates support the idea that our ERL design could potentially be able to induce an $Fe^{II/IV}$ cycle, particularly useful for catalysis with organic substrates.

Ring Chain Isomerism: Ligands for Mediating Two-Electron Reactivity with First-Row Transition Metals

By

Jack Trieu
B.A., Hamilton College, 2011

Advisor: Christopher Scarborough, Ph.D.

A thesis submitted to the Faculty of the
James T. Laney School of Graduate Studies of Emory University
in partial fulfillment of the requirements for the degree of
Master of Science
in Chemistry
2014

Acknowledgements

I would like to thank my P.I., Dr. Chris Scarborough, for accepting me into his lab and giving me the chance to do research under him. Through this experience, I was able to learn more about inorganic chemistry and the concepts that are important to the field. I also thank him not only for his role as a supervisor, but also as a friend.

To my family for always being supportive and believing me. My mom and dad had always been supportive and made sure that I took advantage of all the opportunities available to me. They have always pushed me to become a better person and to continue to learn. I cannot emphasize how grateful I am to them. They both have, and still are, always trying to do the best for me and my sister. It is thanks to them that I have made it this far.

Next, I would like to thank my sister, Jenny Trieu for always believing in me. She has always cheered for me no matter the circumstances. She has always come through for me when things got rough. She is always the one in the crowd yelling and cheering for me the loudest and telling me to do my best. I am grateful to have such a wonderful sister.

I would also like to thank the Scarborough group for the enjoyable times I have had in lab. I would like to thank my committee members, Dr. Simon Blakey and Dr. Frank McDonald for the thoughts and advice they have provided me. I would also like to thank Dr. Cora MacBeth for being supportive and extremely helpful when I turned to her for advice.

The staff and faculty at Emory has helped make my transition to Atlanta significantly easier, especially Steve and Patty from the stockroom. Both of them are

gems to the chemistry department. If it was not for them, I would feel quite lost and homesick. Not only did they provide me with coffee and breakfast, but they also went out of their way to get to know me. I would also like to thank Dr. Wu for always being so quirky and fun to talk to when I needed assistance with the NMR.

In terms of those outside of Emory, I would like to first thank Dr. Nicole L. Snyder and Dr. Joshua Ruppel. The both of them have always been extremely supportive, from the time when I was a sophomore at Hamilton College. It is thanks to them that I became passionate about chemistry. Their passion and their dedication to students are on another level entirely. I am eternally grateful to have met such wonderful mentors.

Next, I would like to thank my friends in Boston. Howard is the first to come to mind. When I first got here, he was the one who made the transition easier for me. He always supported me when I felt like giving up. He was also the first friend from Boston to come down and visit me just to make sure that I was doing well. This man is like a brother to me. Honestly, his friendship and faith in my abilities are unwavering and that is one of the greatest things anyone has ever given me. Another friend I would like to mention is Gregory Karahalis. I initially met him during visitation weekend, and once I came here and got to know him, he quickly became one of my best friends. He has been there for me both in my social and academic life. He has always had my back no matter what happened and listened to my vast amount of venting. Not only that, but he is also one of the most intelligent people I have met and I am confident that we will continue to be friends for a long time.

Table of Contents

List of Figures

List of Tables

List of Schemes

1.0 Introduction

In the past decade, transition metal-catalyzed chemical transformations have become increasingly pertinent to organic synthesis in both academic and industrial settings.[1] Transition metal-catalyzed oxidation reactions have been utilized in industry (e.g. Wacker process)[2,3] and K. Barry Sharpless was awarded the 2001 Nobel Prize in chemistry for his work in this area.[4] However, most of these transition metal-catalyzed oxidation reactions are anaerobic and require expensive and rare late second- or third-row metals (e.g. osmium, ruthenium, palladium)[5], with the exception of the Sharpless' Ti^{IV} epoxidation catalyst and the Jacobsen-Katsuki Mn^{III} epoxidation catalyst (Figure 1).[6]

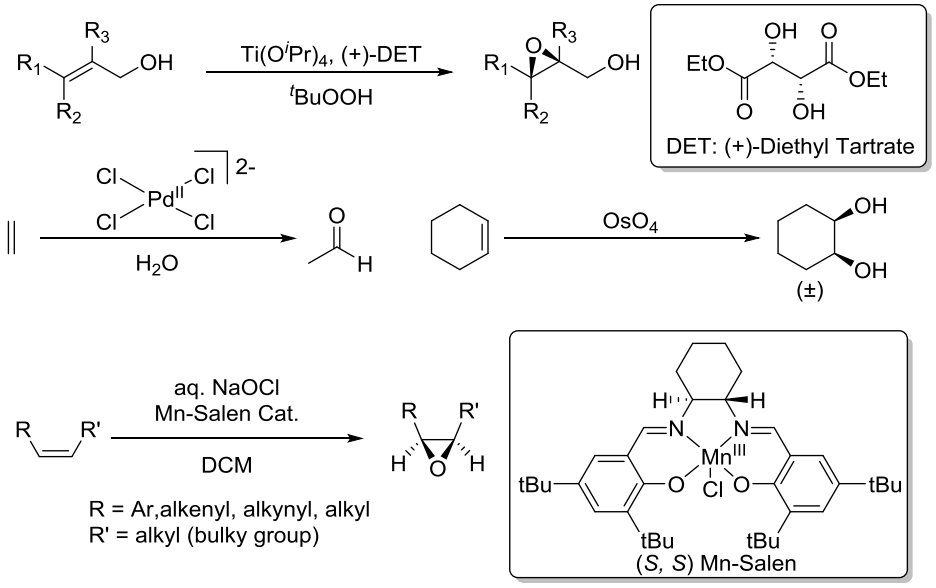

Figure 1. Examples of anaerobic transition metal-catalyzed oxidation reactions.

There has been a drive for the development of transition metal-catalyzed aerobic oxidation systems that employ earth abundant metals and molecular oxygen, as they are more economical and cleaner for the environment.[6] Although there has been some progress in utilizing first-row transition metals for catalysis[7–9], one of the major challenges has been in using first-row transition metals for aerobic oxidation catalysis.

The difficulty with first-row transition metals stems from their poor reactivity and selectivity in organic transformations.[6,7] Currently, most catalytic aerobic oxidation systems require precious metals and high temperatures.[10–14]

Furthermore, the rarity and cost of the late second- and third-row metals makes the development of earth abundant first-row metal catalysts highly desirable.[15] Unfortunately, unlike heavier metals, first-row transition metals have a propensity to perform one-electron processes over the classic two-electron processes inherent to most organic reactions.

The propensity of 3d metals to undergo one-electron processes arises from the relative size of the 3d orbitals. Smaller orbitals interact more weakly with ligand-centered orbitals to give rise to a lower ligand field splitting (Δ_o, Figure 2). Additionally, smaller orbitals lead to an increase in electron-electron repulsion, which is expressed by the Racah B parameter (**B**) shown in Figure 2.[16–18]

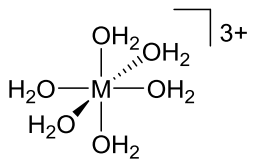

M	D_o (cm^{-1})[a]	Free Ion	B (cm^{-1})[b]
Fe	14000	Fe^{2+}	897
Ru	26500	Ru^{2+}	620

Figure 2. [a] Ligand field splitting energies for Fe^{3+} and Ru^{3+} are displayed.[13,14] [b] Racah B parameters for Fe^{2+} and Ru^{2+} are also shown here, however the B value for Ru^{2+} is not reliable.[12]

In comparison to 3d metals, the inherent nature of both 4d and 5d metals to undergo two-electron processes reflects their success in organic syntheses.[5] Current strategies for inducing two-electron reactivity in late first-row transition metals have primarily been attempted through the use of redox non-innocent ligands.[19,20] Although there has been some recent success with redox non-innocent ligands inducing overall

two-electron reactivity in first-row metals, the success of these systems has been limited.[19–28] In addition, it should be noted that nature is capable of utilizing first-row transition metals, such as iron in cytochrome P450, for organic transformations with high selectivity.[29]

1.1 Electronically Responsive Ligands

The development of first-row metal complexes featuring ligands that can stabilize multiple diamagnetic oxidation states has been considered a viable option for the catalysis of organic transformations.[20] If a ligand is able to accommodate changes in metal oxidation states by altering the electronic structures of its coordinating atoms, the two-electron reactivity of the late second- and third-row metals should be viable for the late first-row metals. Currently in coordination chemistry, only a few ligands[20] are able to induce two-electron reactivity in first-row transition metals, while most ligands[7,30] only support first-row transition metals as they undergo one-electron changes in oxidation state.

The spectrochemical series can aid in designing ligands capable of promoting two-electron reactivity in first-row transition metals (Figure 3). π-Acceptor and π-donor ligands are preferred in such a design, as they are tuneable and can be potentially modified to interconvert between π-acceptor and π-donor (e.g. imine to amido), making them better able to stabilize high and low valent first-row metal oxidation states, respectively.

Spectrochemical Series : π-donors (left) to π-acceptors (right)
Halogens < -OH < H_2O < H_3CCN < py < bpy < PPh_3 < CO

Figure 3. Spectrochemical series showing donors and acceptors from left to right.[31]

Some of the classic π-acceptors used in organometallic chemistry are phosphine (PR_3) ligands. Phosphine ligands are commonly used in palladium catalysis due to their ability to stabilize the low valent Pd^0 center; once oxidized to Pd^{II}, they become more labile and are subsequently replaced by stronger π- and σ-donors.[32] Strong π-donors, such as oxos[33–35] and imidos[36], are expected to stabilize high valent metal centers. However, oxos and imidos are unable to behave as π-acceptors and therefore unable to stabilize low valent metals. In order to stabilize both high and low valent metal oxidation states, the ligand needs to access both π-donor and π-acceptor chelates. Instead of relying on labile or oxidizable ligands, the ligand platform should be able to interconvert between a strong π-donor and π-acceptor in response to changes in metal oxidation states.

Herein, the desired novel ligand designs are distinguished by the incorporation of functional groups capable of tautomerism, and therefore have the potential to interconvert between π-donor and π-acceptor modalities. These ligand platforms, which undergo ring-chain isomerism in response to changes in the metal oxidation states via two-electron processes, will be referred to as electronically responsive ligands (ERLs, Figure 4)

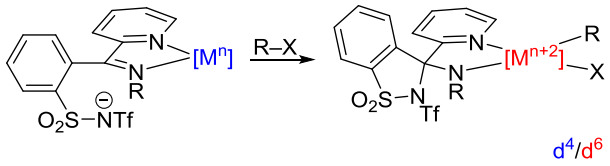

Figure 4. Proposed ERL for stabilizing d^4/d^6 metal.

The research reported here will be on the progress towards observing d^4/d^6 ERL complexes with emphasis on $Fe^{II/IV}$ centers (Figure 4).

1.2 Design of ERLs for $Fe^{II/IV}$ Stabilization

The effective ERL design must incorporate components that can interconvert to stabilize both Fe^{II} and Fe^{IV} centers. Generally, Fe^{II} centers are stabilized by π-acceptors (e.g. α-diimines)[37], while Fe^{IV} complexes are stabilized by π-donor ligands (e.g. amidos).[33,38,39]

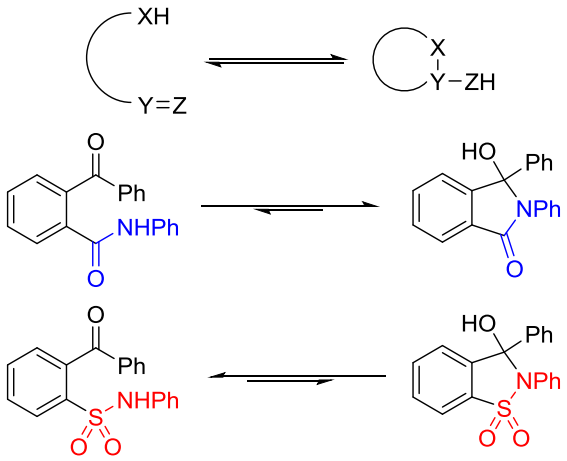

Figure 5. Examples of compounds that exhibit RCT. Anilide (blue) is more nucleophilic than a sulfonamide (red) as sulfonyls are generally more electron-withdrawing than carbonyls.[40–42]

The ERL requirements for stabilizing Fe^{II} and Fe^{IV} comes from the concept of ring-chain tautomerism (RCT, Note: RCT is analogous to ring-chain isomerism).[43,44] RCT was first proposed by Larr and coworkers and was used to describe a compound bearing a weak nucleophile and an electrophilic π-system that is interconverting between a chain and ring form (Figure 5).[43,44] There are two requirements for a compound to exhibit RCT: a functional group with polarized multiple bonds (e.g. C=N, C=O, C=S) and another functional group that behaves as a weak nucleophile. Some examples of organic compounds that exhibit such properties are shown in Figure 5 with an anilide favoring the ring form. In contrast, an aryl sulfonamide, a weaker nucleophile due to the more electron-withdrawing sulfonyl group, is shown to favor the chain form.[40–42]

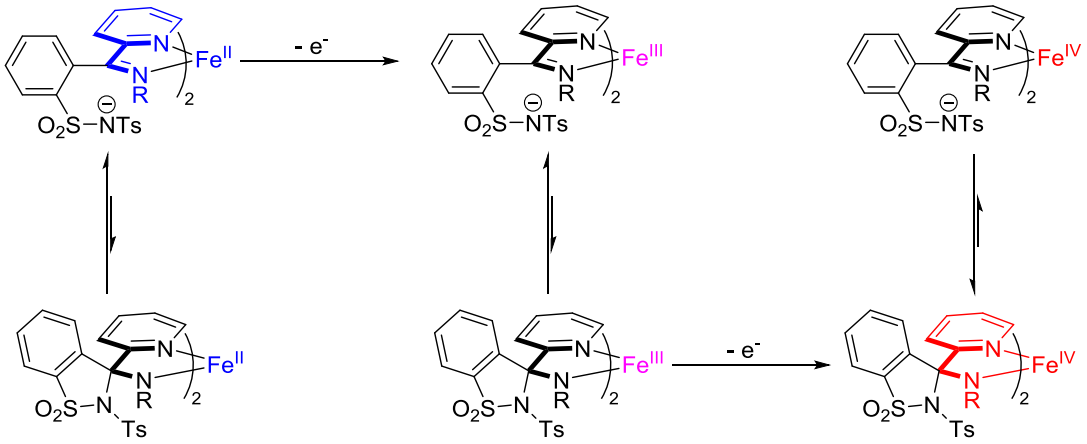

Figure 6. Hypothesized reactivity of ERLs acting on Fe^{II}, Fe^{III}, and Fe^{IV} centers.

The ERL design applies the RCT concept to metal complexes, where the ligand's chain and ring forms are dependent on the changes in metal oxidation states. The proposed ligand design meets the electronic needs of Fe^{II} and Fe^{IV}: in the Fe^{IV} state, the imine functionality (π-acceptor) should isomerize to the amido functionality (π-donor) via a ring-closing nucleophilic attack by the pendant sulfonimidate (Figure 6). The π-accepting imino-pyridine platform should favor Fe^{II} over Fe^{III} because Fe^{II} is more electron rich. Conversely, the π-donating amido-pyridine platform should favor Fe^{IV} over Fe^{III} because it is more electron poor. Ideally, the ligands should stabilize the Fe^{II} and Fe^{IV} centers in the chain and ring form, respectively, and effectively destabilize the Fe^{III} center because of the electronics of the metal oxidation states (Figure 6).

The ERLs' interconversion between chain and ring forms is highly dependent on the nucleophilicity of the pendant amide. Additionally, the potential of the pendant amide coordinating to the metal center must be considered. Weakly donating pendant amides, such as triflamidates, was used to avoid competitive coordination to the metal center.[45] The spectrum of pendant amides covered spans from sulfonyl triflimidate (reference pK_a, $F_3CSO_2NH_2$ = 9.7 in DMSO) to sulfonyl phosphamidate (reference pK_a,

$(MeO)_2P(O)NHPh$ = 18.4 in DMSO).[36,46,47] To control for the nucleophilicity of the pendant amide, a broad range of pK_a values must be explored to determine the ideal amide nucleophile that can induce cyclization for an Fe^{IV} center (Figure 7).

After the Fe^{II}-ERLs were successfully synthesized and characterized, the next study investigated the redox properties and O_2 reactivity of the Fe^{II}-ERL species to determine how the ERL responds to changes in metal oxidation state. The redox and reactivity studies will have implications for future development of first-row transition metal catalysts for oxidative transformations (e.g. alcohol oxidation[10–14]).

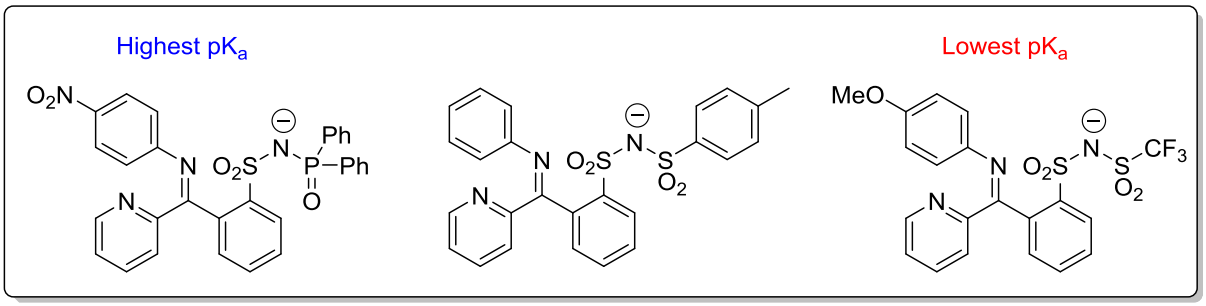

Figure 7. Target ERLs.

1.3 Goals of Project

The goals of this project are as follows:

1. Develop a viable synthetic route for the desired ERLs (Figure 8).

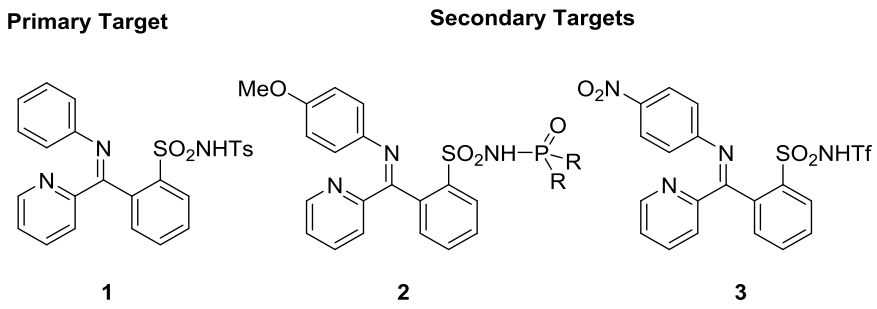

Figure 8. Current ERL targets.

2. Conduct structural characterization studies of the $Fe(ERL)_2$.
3. Perform reactivity studies of the $Fe(ERL)_2$ (Scheme 1).

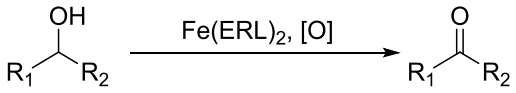

Scheme 1. Aerobic oxidation by $Fe(ERL)_2$

2.0 Results and Discussion

2.1 *o*-Lithiation of Aryl Sulfonate ERL Synthesis Route

Initially, the most desirable synthetic route for the ERLs was the *o*-lithio aryl sulfonate addition of 2-pyridinecarbonitrile followed by the addition of thionyl chloride to afford **5** (Scheme 2). [48]

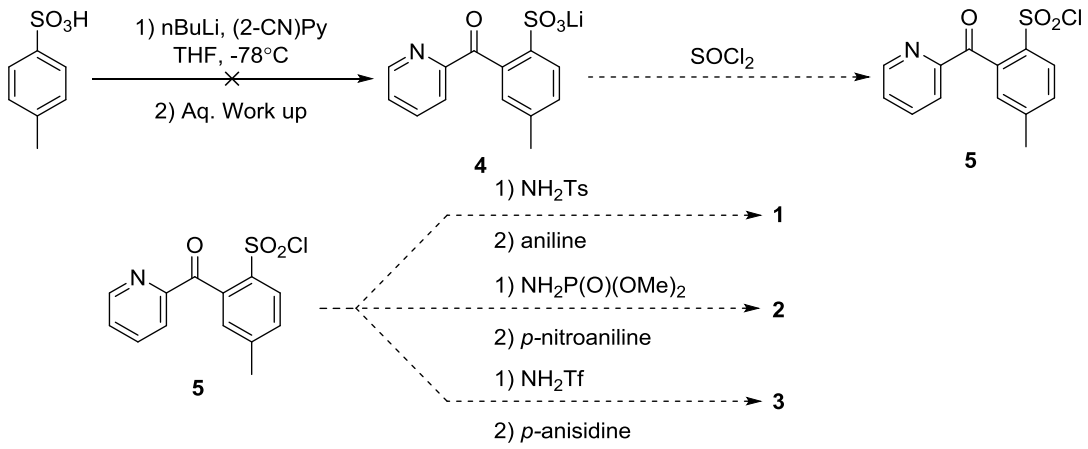

Scheme 2. Proposed synthesis to ERL **1** via the key intermediate **5.**

If compound **5** is successfully synthesized, then it can be treated as a key intermediate to access ERLs **1**-**3** (Scheme 2). Currently, there are only two known procedures on *o*-lithiations of aryl sulfonates.[48,49] Both *o*-lithiation procedures were attempted and yielded no products (Scheme 2). Instead, starting material was recovered from both reaction mixtures. Although previously reported procedures were known, an alternative synthesis was attempted due to unsuccessful results

2.2 ERL Syntheses *via* Pyridyl Additions to Saccharin Derivatives

A three-step synthesis for the ERLs is shown in Scheme 3, with the key step being a pyridyl Grignard addition to tosyl saccharin.[50]

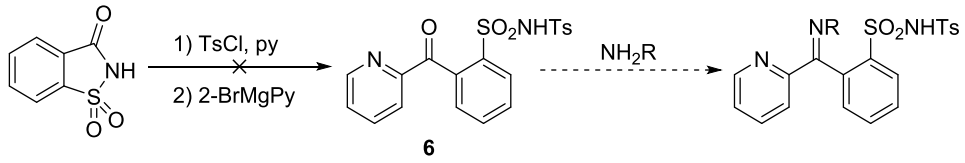

Scheme 3. Grignard addition to Ts-saccharin to afford **6**.

Initially, the tosyl saccharin synthesis appeared straightforward. The tosyl saccharin was characterized through ^{1}H and ^{13}C NMR spectroscopy, and only slight differences were observed in the spectra compared to saccharin. Moving forward, however, the following step did not generate the desired **6** (Scheme 3). Instead, multiple resonances were seen in place of the expected singlet for the benzylic protons of the tosyl moiety (~2.20 ppm) in the ^{1}H NMR, suggesting the starting material was not tosyl saccharin. In addition, mass spectrometry did not support the presence of tosyl saccharin, reiterating that tosyl saccharin had not been successfully synthesized. Instead, the mass spectrometry revealed the majority of the starting material was retained.

In 2004, Knochel and coworkers developed the turbo Grignard reagent, which was shown to be more nucleophilic and less basic than the typical Grignard reagent.[51] A new synthesis was attempted, which involved a pyridyl turbo Grignard addition to saccharin to obtain the free sulfonamide **8** (Scheme 4).

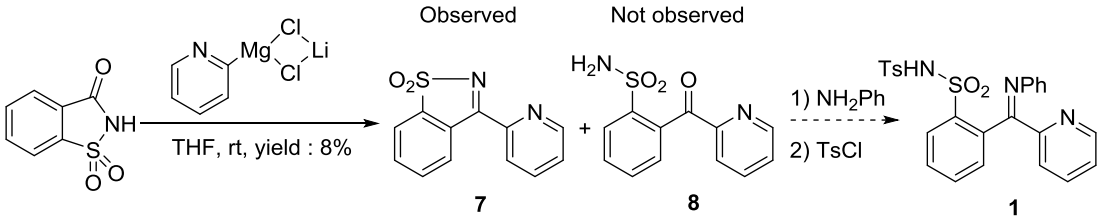

Scheme 4. New ERL synthesis utilizing turbo Grignard.

Instead of generating **8**, the pyridyl turbo Grignard addition to saccharin produced compound **7** in 8% yield (Scheme 4). Initially, **7** seemed promising for potential transimination to generate compound **9**. To this end, various transimination procedures were attempted on compound **7** (Table 1).[56]

Table 1. Different transimination conditions for **7**.

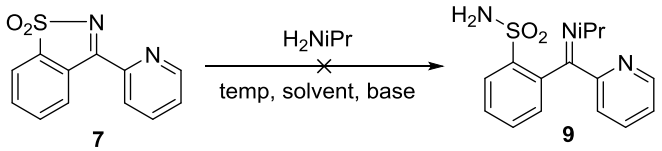

Entry	Base	LA	Temp(°C)	Solvent	Yield (%)
1	-	$TiCl_4$	rt	THF	0*
2	iPrMgCl	-	80	Et_2O	0*
3	-	-	80/100	neat	0/0*
4	nBuLi	-	-78→rt	THF	0*
5	-	$ZnCl_2$	80	AcOH/MeOH	0*

-LA: Lewis Acid

[a] *p*-toluidine was used

*>95% starting material retained

Unexpectedly, all of the reaction conditions attempted returned compound **7**, suggesting that it is inert to transimination (Table 1). Given that the transimination attempts failed to generate **9**, a different synthetic route was pursued.

In scheme 5, saccharin is alkylated with benzyl bromide to afford the benzyl saccharin, followed by a subsequent pyridyl turbo Grignard addition to generate **10**, a key

intermediate that can access ERLs **1**-**3**. The pyridyl turbo Grignard addition to benzyl saccharin afforded the desired **10**, albeit in 20% yield (Scheme 5).

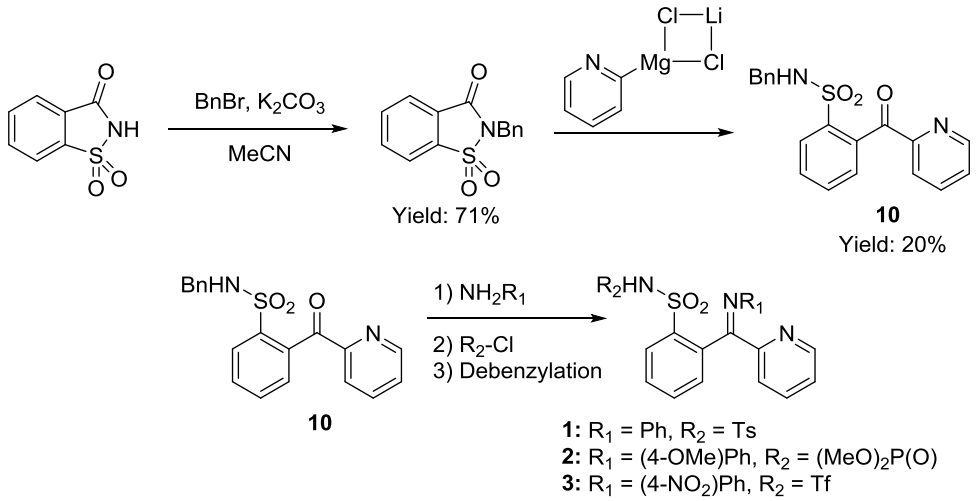

Scheme 5. New proposed synthesis of ERLs **1-3** from saccharin.

The ^{1}H NMR spectrum of **10** consists of two related sets of benzylic resonances (Figure 9). While the doublet at 4.24 ppm is indicative of **10**, there are another two doublets at 4.29 and 4.48 ppm potentially indicative of another isomer of **10** (Figure 9). The ^{13}C NMR spectrum of **10** has two resonances that are consistent with a ketone carbon (196.3 ppm) and a non-aromatic quaternary carbon (87.9 ppm) (Figure S5). In addition, there are two related benzylic carbon resonances at 47.6 and 41.9 ppm. DEPT spectroscopic analysis of **10** confirms the presence of both ketone carbon and quaternary carbon resonances by their absence in the spectrum (Figure S6).

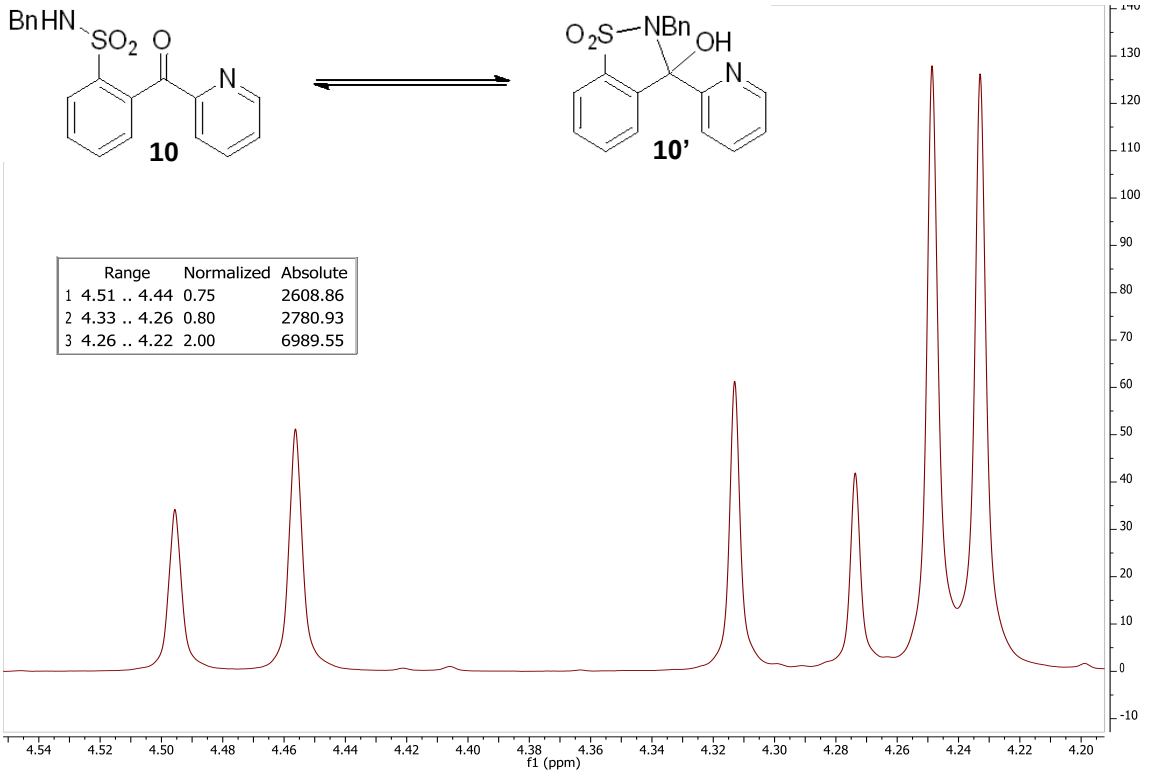

Figure 9. Key ^{1}H NMR peaks from **10** that support the compound displays RCT. The doublet at 4.24 ppm correlates to the chain **10** and the other set of doublets at 4.29 and 4.48 ppm correlates to the ring **10'**.

^{1}H NMR spectroscopic analysis of **10** indicates that the substrate exhibits RCT (1:0.8, Figure 9). The two related sets of benzylic resonances are suggestive of chain **10** and ring **10'** (Figure 9). Chain **10** is most consistent with the doublet at 4.24 ppm with a *J*-coupling constant of 8 Hz. The doublet is likely to be the result of the benzylic protons coupling to the neighboring sulfonamide proton. The two doublets at 4.29 and 4.48 ppm have unusually high *J*-coupling constants of 20 Hz, suggesting those particular protons are structurally locked. The high *J*-coupling constants may be the result of the steric hindrance brought on by the intramolecular cyclization of the benzyl sulfonamide onto the ketone. Based on the ^{1}H NMR data and the proposed sulfonamide cyclization, ring **10'** is the most consistent with the two doublets at 4.29 and 4.48 ppm.

A similar reaction was attempted with benzyl phthalimide and generated only the ring product **10''**. The ^{1}H NMR spectrum of **10''** has two doublets at 4.57 and 4.89 ppm with *J*-coupling constants of 20 Hz, consistent with the two resonances and high *J*-coupling constants seen in **10** (see SI).

^{13}C NMR spectrum of **10** also provides evidence of **10** exhibiting RCT. The carbonyl resonance at 196.3 ppm is associated with **10** and a quaternary carbon resonance at 87.9 ppm is likely to be associated with **10'** (Figure S5). Based on the chemical shift, the quaternary carbon of **10'** is likely to be bonded to the alcohol. The DEPT analysis reiterates that **10** contains both a ketone carbon and a non-aromatic quaternary carbon, which further corroborates **10** exhibits RCT.

Furthermore, the pyridyl turbo Grignard addition to benzyl saccharin generated exclusively compound **10** under these conditions. The absence of side products could be the result of compound **10** undergoing RCT. Unlike previous substrates, the specific nucleophilicity of the benzyl sulfonamide of **10** may have prevented the second pyridyl addition (Scheme 6).

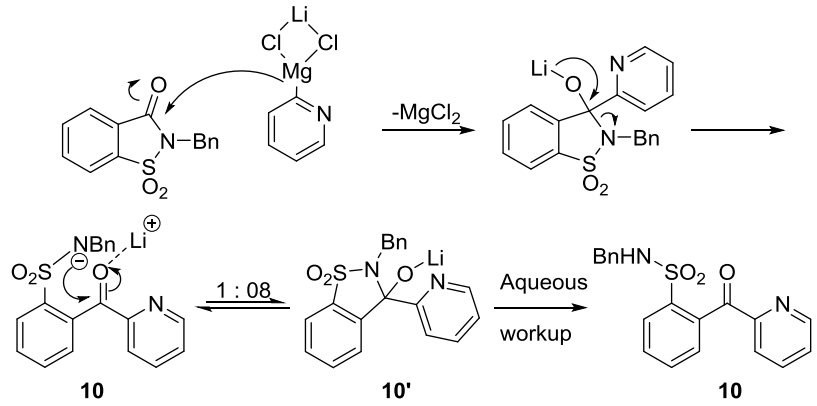

Scheme 6. Proposed mechanism of the formation of **10**.

When compound **10** is generated after the first pyridyl addition, it is possible the benzyl sulfonamide cyclized onto the electrophilic ketone to generate **10'** (Scheme 6). Once **10'** is formed, **10** is protected from the second pyridyl addition as intramolecular reactions generally occur faster than intermolecular reactions. Then, compound **10** is obtained upon an aqueous workup. Compared to previous syntheses, this route is able to generate **10,** a compound that exhibits RCT. The observed RCT in **10** is promising because it suggests that the ERLs will perform as predicted when metallated.

In the next step of this synthesis, an amine condensation reaction is shown in Scheme 7.

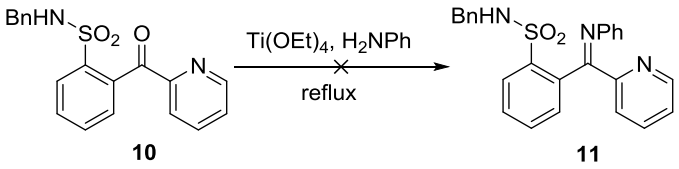

Scheme 7. Amine condensation of **11**.

Compound **10** was placed in known conditions for titanium-promoted imine formation (Scheme 7).[52] Unfortunately, even under harsh conditions the reaction did not produce the desired imino-pyridine **11**.[52] Instead, **10** was fully recovered. This suggests that $Ti(OEt)_4$ was not an effective lewis acid and dehydrating reagent to catalyze convert compound **10** to the desired imino-pyridine **11**.

$TiCl_4$ was used as an alternative lewis acid and dehydrating reagent for the amine condensation. Using $TiCl_4$ to catalyze the amine condensation onto **10**, the reaction afforded **11a** in 34% yield (Scheme 8).[53]

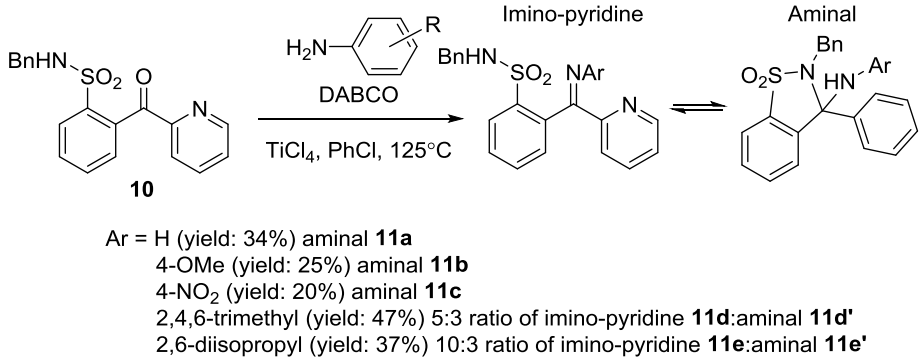

Scheme 8. $TiCl_4$-promoted imine formation for compounds **11a-e**.

However, ^{1}H NMR, ^{13}C NMR, and infrared spectroscopic analyses of **11a** show that the primary form of the product is the cyclic aminal **11a**. Unlike compound **10**, the ^{1}H NMR spectrum of **11a** consists of only one set of benzylic resonances, where both doublets at 4.27 and 4.38 ppm are analogous to the benzylic resonances observed for **10'**. The two doublets of **11a** at 4.27 and 4.38 ppm display high *J*-coupling constants of 15.4 Hz, comparable to values seen in **10'**. Similar to compound **10**, a quaternary carbon resonance is observed at 80.4 ppm in the ^{13}C NMR spectrum of **11a**. However, no imine or ketone carbon was observed. The carbon resonance at 80.4 ppm is indicative of a carbon bonded to an amine. The presence of a quaternary carbon resonance at 80.4 ppm and the absence of an imine carbon resonance suggest that **11a** is likely to be in a ring form. Infrared spectrum of **11a** only shows an N-H stretch at 3329 cm^{-1}. The infrared spectrum supports the aminal **11a** due to the presence of an N-H stretch at 3329 cm^{-1} and absence of an imine stretch around 1670 cm^{-1}. Exclusive observation of the aminal **11a**

suggests that even if the imine is formed, the sulfonamide's proton may be acidic enough to promote cyclization to generate the observed aminal compound **11a**.

To study the electronic and steric effects on RCT in this compound, a variety of aniline derivatives were employed for the amine condensation reaction. *p*-Anisidine and (*p*-nitro)aniline were used and exclusively generated aminals **11b** and **11c**, which demonstrated that electronics do not have a strong influence on the formation of the desired imino-pyridine platform. However, when sterically hindered anilines were used, such as 2,4,6-trimethylaniline and 2,6-diisopropylaniline, the equilibrium shifted in favor of the imino-pyridine (Figure 10). ^{1}H NMR and ^{13}C NMR spectroscopic analyses also revealed **11d** and **11e** to have two related sets of resonances and *J*-coupling constants consistent with those observed in **10** (see SI).

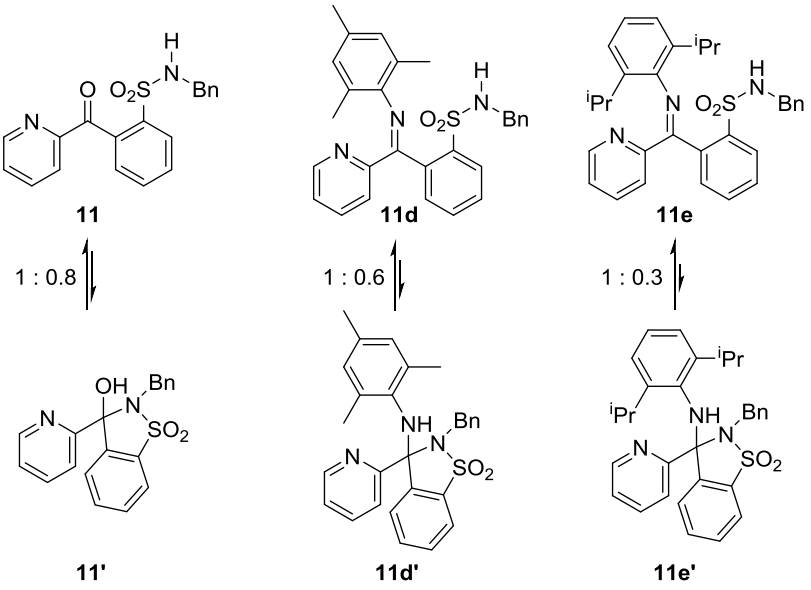

Figure 10. Sterics are shown to favor the imino-pyridine form. Ratios were determined via ^{1}H NMR spectroscopy.

Although compound **11e** has an imino-pyridine:aminal ratio of 1:0.3, it is not the preferred ligand for metallation due to the steric bulk of the diisopropyl groups (Figure

10). If the aryl imine is too sterically hindered, then it could potentially inhibit the nucleophilic attack of the sulfonimidate onto the imine when the metal is oxidized and prevent the metal oxidation induced ring-chain isomerism.

In the next step of the synthesis, **11d** was treated under basic conditions in the presence of tosyl chloride. The desired tosylated product **12d** was obtained in 40% yield (Scheme 9).

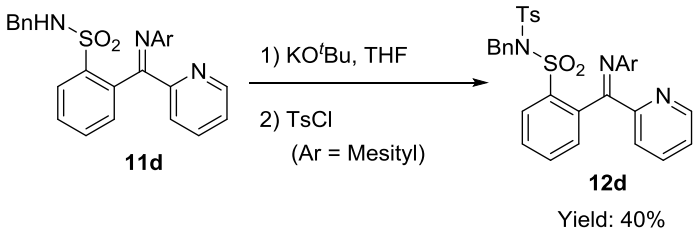

Scheme 9. Tosylation of benzyl sulfonamide **11d**.

Similar to **10** and **11d**, the ^{1}H NMR spectrum of **12d** consists of two related sets of benzylic resonances (Figure 11). While the singlet at 4.53 ppm is indicative of **12d**, there are two doublets at 4.49 and 4.77 ppm potentially indicative of another isomer of **12d**. The ^{13}C NMR spectrum of **12d** shows an imine carbon resonance at 168.1 ppm and two related benzylic carbon resonances at 52.2 and 44.7 ppm (see SI).

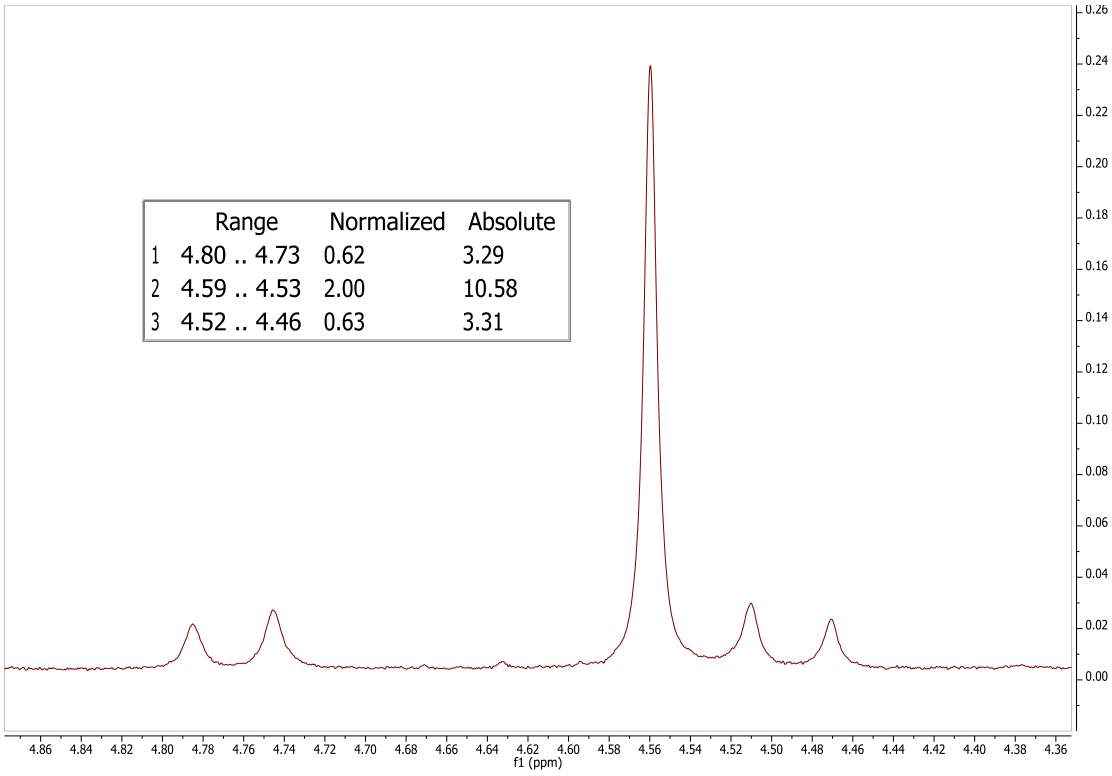

Figure 11. ^{1}H NMR of **12d** showing the diagnostic benzyl proton resonances. The singlet at 4.56 ppm is suggestive of an imino-pyridine **12d**, while the two doublets at 4.49 and 4.77 ppm are suggestive of an aminal **12d'**.

^{1}H NMR spectroscopic analysis of **12d** suggests it exhibits ring-chain isomerism (1:0.3, Figure 11). A comparison between the benzylic resonance of **11d** at 4.01 ppm and the benzylic resonance at 4.56 ppm suggests compound **12d** is consistent with the singlet at 4.56 ppm. The sulfonimide of **12d** should deshield the neighboring benzylic protons further downfield than the sulfonamide of **11d** due to its stronger electron-withdrawing nature. In addition, the benzylic protons of **12d** are expected appear as a singlet in the ^{1}H NMR when the sulfonamide is tosylated. The two doublets at 4.49 and 4.77 ppm are analogous to the benzylic resonances observed in isomers **10'** and **11d'** (see SI). Both doublets at 4.49 and 4.77 ppm have *J*-coupling constants of 16 Hz, which are comparable to the values seen in compounds **10'** and **11d'** (see SI). However, compound **12d** does

not have a proton for RCT. This suggests that **12d** exhibits N-benzyl migration, interconverting between the chain **12d** and the putative ring **12d'** (Figure 12).

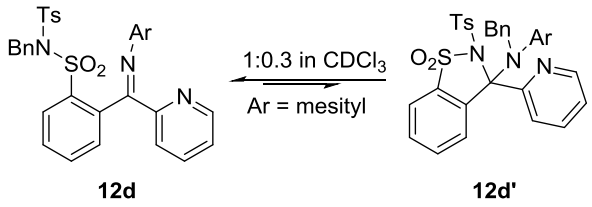

Figure 12. Proposed equilibrium of compound **12d** and **12d'**.

^{13}C NMR spectroscopic analysis supports that compound **12d** displays N-benzyl migration. Unlike **10** and **11d**, only the imine carbon resonance indicative of **12d** is observed at 168.1 ppm in the ^{13}C NMR spectrum. Although the non-aromatic quaternary carbon of **12d'** is not observed, two related benzylic carbon resonances are observed at 52.2 and 44.7 ppm. The resonance at 52.2 ppm is associated with **12d** because the benzylic carbon should be further downfield due to the electron-poor sulfonimide. In contrast, the other carbon resonance at 44.7 ppm suggests that the benzylic carbon is in a different chemical environment, likely to be bonded to the amine of **12d'**. The proposed **12d'** is the most consistent with the resonance at 44.7 ppm because the amine, a more electron-rich group, should shift the benzylic resonance further upfield.

A comparison to the benzylic carbon resonance of the precursor **11d** at 48.0 ppm also corroborates that **12d** and **12d'** correspond to the resonances at 52.2 and 44.7 ppm, respectively. **12d** is associated with the carbon resonance at 52.2 ppm because the sulfonimide, a stronger electron-withdrawing group than the sulfonamide, should shift the benzylic resonance further downfield. In contrast, **12d'** is consistent with the carbon resonance at 44.7 ppm because the amine, a stronger electron-donating group than the

sulfonamide, should shift the benzylic resonance further upfield. The ^{13}C NMR spectrum of **12d** supports that **12d'** is the other isomer that is in equilibrium with **12d**.

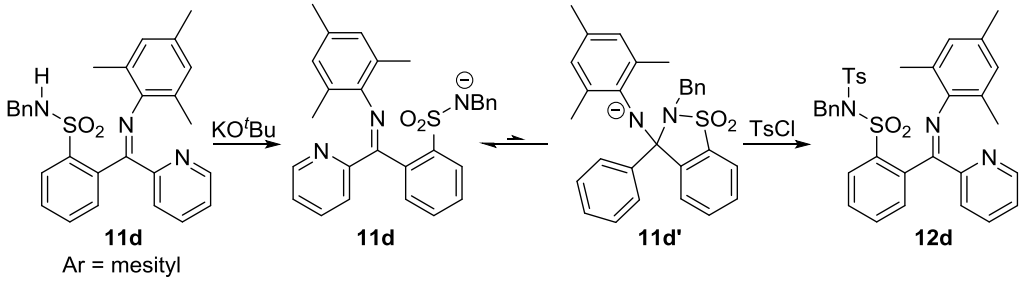

Scheme 10. Proposed mechanism of the formation of **12d**.

The tosylation of **11d** only generated **12d,** suggesting the equilibrium favors the imino-pyridine **11d** under basic conditions (Scheme 10). The cyclization of the sulfonamide under basic conditions may have been inhibited by the methyl groups of the (2,4,6-trimethylphenyl)imine, which can cause the anion to be primarily localized on the sulfonamide. As a result, the sulfonamide may have been the only nucleophilic site available for tosylation. This may explain why **12d** was the only product observed.

To further investigate the identity and properties of **12d**, ^1H NMR spectra were obtained in two different solvents, chloroform-*d* and methanol-d_4, to determine if solvent polarity can influence the ratios of the benzylic resonances. If the ratio of the benzyl resonances changes, that would suggest the **12d** exhibits N-benzyl migration. If the ratio does not change, that would suggest **12d** is unlikely to be exhibiting N-benzyl migration.

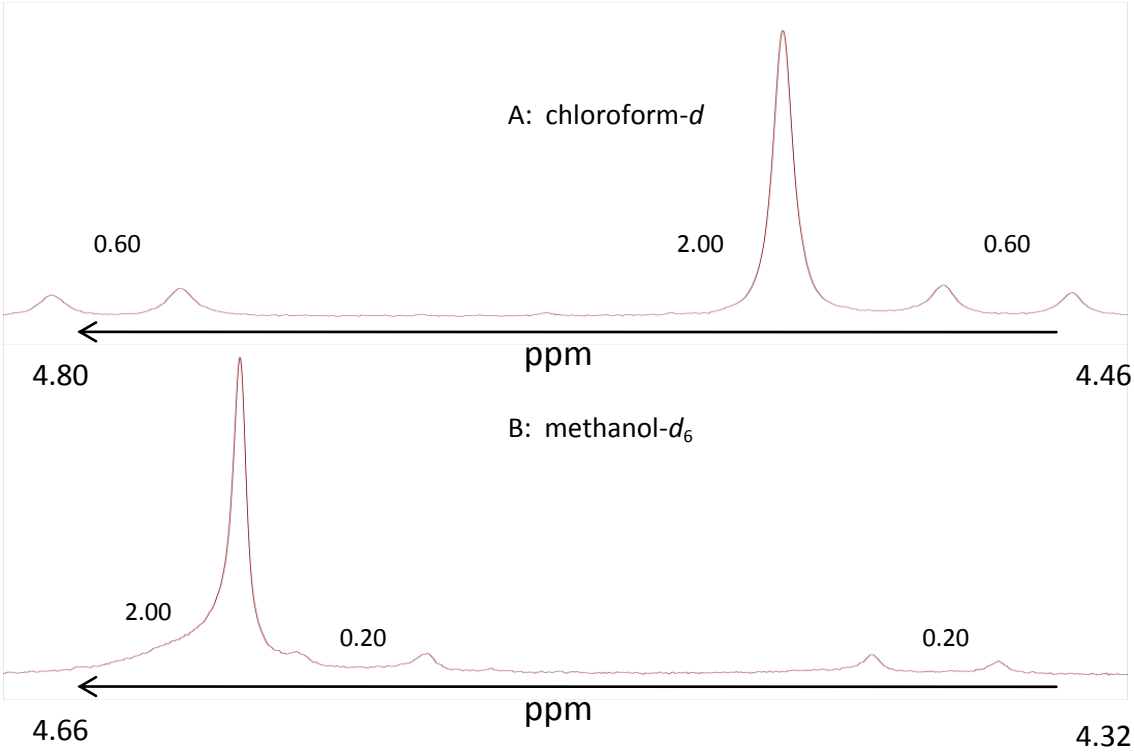

Figure 13. A) **12d** in chloroform-*d* shows a ratio of 1:0.6 of **12d**:**12d'**. B) **12d** in methanol-d_4 shows a ratio of 1:0.2. Resonances were integrated in reference to the mesityl aromatic protons that show up at 6.76 ppm.

When **12d** was dissolved in methanol-d_4, the ratio of **12d**:**12d'** changed from 1:0.6 in chloroform-*d* to 1:0.2 in favor of the imino-pyridine **12d** (Figure 13). The effect of solvent polarity on both sets of benzylic resonances are associated with a single compound, suggesting **12d'** exists in equilibrium with **12d**. Namely, the solvent-dependency of compound **12d** is consistent with reversible N-benzyl migration concomitant with ring-chain isomerism between **12d** and **12d'**. This result may shed light upon the absence of the quaternary carbon of **12d'** in the ^{13}C NMR spectrum. Quaternary carbons already display characteristically low signals, which may be exacerbated by the observation that it exists as the minor equilibrium structure **12d'**.

In addition, variable temperature ^{1}H NMR (VT NMR) spectroscopic studies support that **12d** exhibits N-benzyl migration. When compound **12d** was dissolved in

DMSO-d_6, the VT NMR data reveal that the singlet at 4.74 ppm and the two doublets at 4.51 and 4.68 ppm coalesce into a broad singlet in at elevated temperatures (Figure S7). At room temperature (22.1 ºC), the diagnostic benzylic resonances for **12d** and **12d'** are observed (Spectrum 3, Figure S7). When the temperature is increased to 50 ºC, the singlet of **12d** and the two doublets suggestive of **12d'** begin to broaden (Spectrum 2, Figure S7). At 80 ºC, there is a complete coalescence of the benzylic resonances at 4.71 ppm (Spectrum 1, Figure S7). Following, the same sample is cooled to room temperature and spectrum 3 is obtained again with the reappearance of the singlet at 4.74 ppm and the doublets at 4.51 and 4.68 ppm (Spectrum 3, Figure S7).

The coalescence and reappearance of the singlet and doublets are indicative of reversible N-benzyl migration between **12d** and **12d'**. Furthermore, the VT NMR data support the potential of ERLs exhibiting ring-chain isomerism in response to the changes in metal oxidation states. However, more studies need to be done to establish the reversible N-benzyl migration.

In this study, we were able to develop a rational synthesis for **12d**, the precursor to ERL **1**. Although the synthesis is focused on **1**, it is also capable of affording ERLs **2** and **3** through the key intermediate **11**. Through this synthesis, spectroscopic data support that compounds **10**, **11d**, and **11e** exhibit RCT. Spectroscopic analysis of compound **12d** also reveals that it exhibits reversible N-benzyl migration, a phenomenon that has not been reported in the literature. These observations of compounds displaying ring-chain isomerism reiterate the potential of ERLs inducing two-electron reactivity in first-row transition metals. Unfortunately, the ligand synthesis is not scalable and requires further

optimization. As a result, the lack of materials made studies on the desired metal complexes difficult (see Appendix).

2.3 Syntheses and Metallation of Alternative Ligands

Due to the low-yielding synthesis of **12d**, alternative ligands that were more synthetically accessible were pursued (Figure 14).

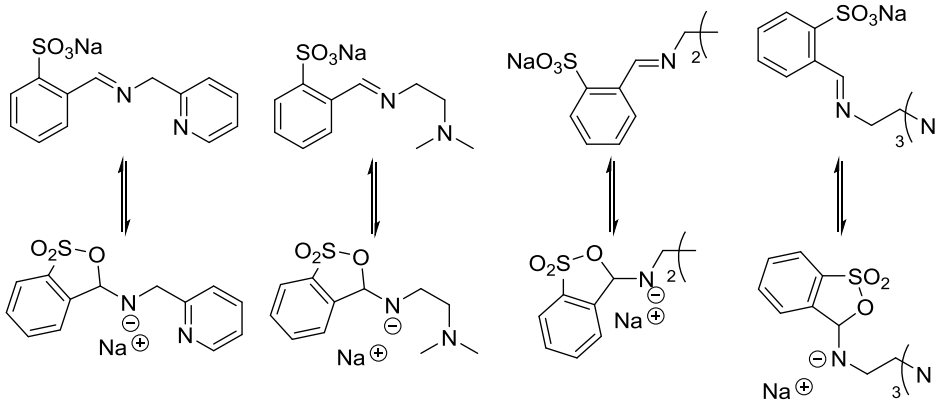

Figure 14. Proposed ligand platforms with their chain and ring forms, where the sterically hindered sulfonimidate is replaced with a sulfonate.

In these new ligand platforms, the sterically hindered pendant sulfonimidate is sacrificed for a sulfonate for the conversion of the π-acceptor imine to the π-donor amido ligand (Figure 14). The drawback to the sulfonate is that it is a weaker acid than a sulfonimidate and therefore a better nucleophile and ligand, making it more likely to coordinate to the metal center.[54] Like the proposed ERLs **1-3**, these ligand platforms also have the potential to form a polymeric network and three potential bidentate chelates, five-membered, six-membered, and also a seven-membered chelate. Another drawback to these ligand designs is that the aldimines are expected to be more susceptible to hydrolysis than the ketimines in the original ERL designs **1-3**. Although these ligands have many drawbacks, they could potentially help establish the ERL concept. The ligands were synthesized in good yields through a one-step scalable route and the reaction

conditions were extended to a variety of primary amines to produce a new ligand series, **13-16** (Scheme 11).

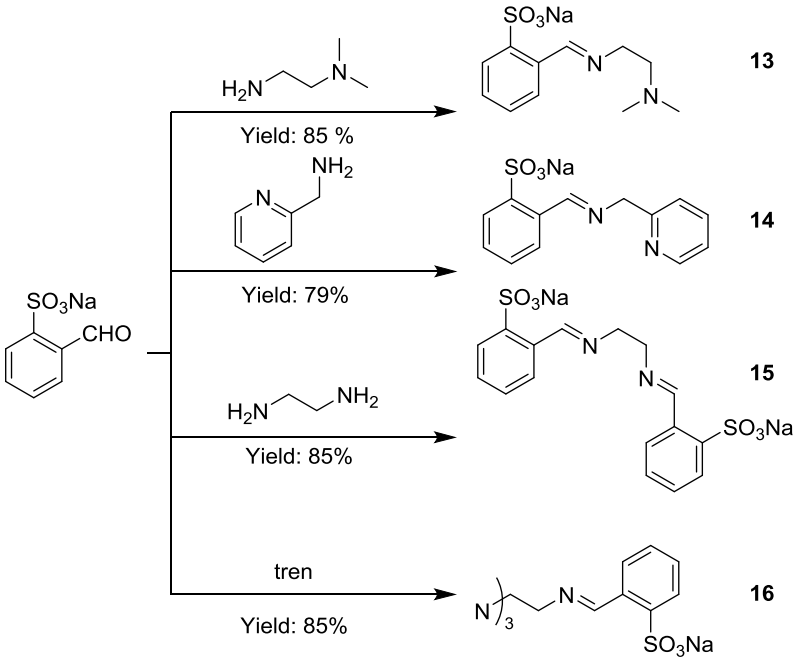

Scheme 11. One-step synthesis to the new ligand platforms.

Once synthesized, it was found that the new ligand platforms **13-16** did not exhibit ring-chain isomerism like compounds **10**, **11d**, **11e**, and **12d**, potentially due to the ligands being sodium salts rather than protonated ligands. These new ligands **13-16** were able to address whether the ligands would chelate to the metal center via a five-, six-, or seven-membered chelate or form a polymeric network.

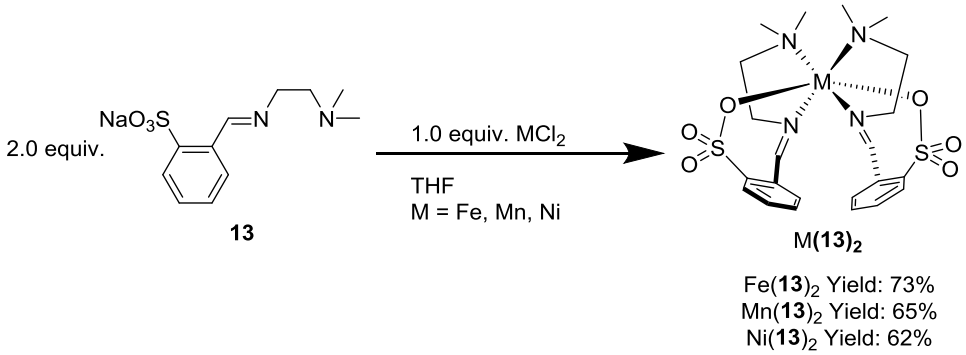

Scheme 12. Metallation of **13** onto MCl_2.

Metallation of ligand **13** was achieved by dissolution of the 2.0 equivalents of **13** in tetrahydrofuran followed by treatment with 1.0 equivalent of $FeCl_2$ (Scheme 12). Subsequent removal of NaCl salts afforded the desired Fe(**13**)$_2$ complex in 73% yield.

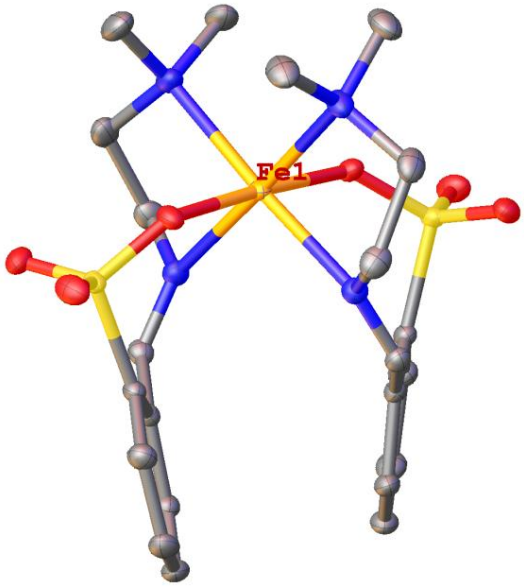

Figure 15. X-ray crystal structure of Fe(**13**)$_2$. Hydrogens are omitted for clarity.

X-ray crystal structure determination of Fe(**13**)$_2$ reveals that in addition to the expected bidentate chelation, the sulfonates are able to bind to the metal center in the axial position *trans* to one another, yielding a six-coordinate Fe^{II} complex (Figure 15).

Under the same conditions as Fe(**13**)$_2$, the Mn^{II} and Ni^{II} six-coordinate species were also generated using $MnCl_2$ and $NiCl_2$ (Scheme 12). X-ray crystal structure determination reveal both Mn^{II} and Ni^{II} complexes are isostructural to Fe(**13**)$_2$ (Figure 16).

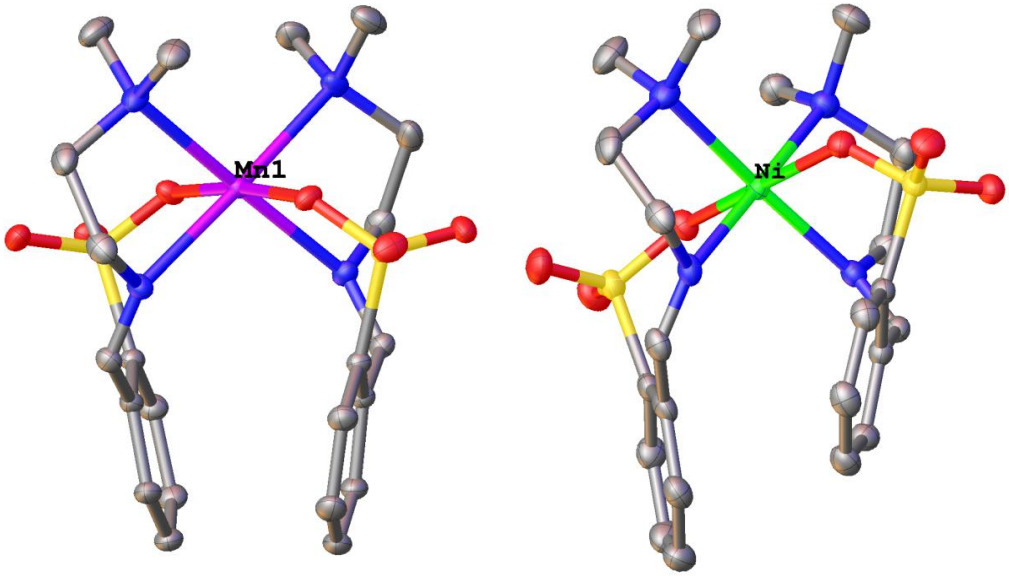

Figure 16. X-ray crystal structures for Ni(**13**)$_2$ and Mn(**13**)$_2$. Hydrogens are omitted for clarity.

The complexes addressed whether the sulfonates would or would not coordinate the metal center. X-ray crystal structure determination of the Fe^{II}, Mn^{II}, and Ni^{II} complexes reveals both sulfonates coordinating to the metal centers axially (Figures 15 and 16). The coordination of the sulfonates is most likely due to the electrostatic interactions between the anionic oxygen of the sulfonate and the cationic metal center.

The complexes also addressed whether the ligands would favor the *cis* coordination of the amines to relieve the system of the *trans* effect or *trans* coordination of the amines to reduce steric strain from the methyl groups of the amines. Crystal structures of the Fe^{II}, Mn^{II}, and Ni^{II} complexes reveal that the *cis* coordination of the amines is favored as it relieves the complexes of the *trans* effect (Figures 15 and 16).

Although a cobalt complex was generated using $CoCl_2$ under the same conditions as Fe(**13**)$_2$, the compound that was isolated was a dimeric species [(**13**)$_2$$Co^{II}_2$($\mu$-Cl)$_2$]

(Figure 17). The unexpected dimeric [(**13**)$_2$Co$^{II}_2$(μ-Cl)$_2$] could have resulted from the addition of an extra equivalent of $CoCl_2$. Even though [(**13**)$_2$Co$^{II}_2$(μ-Cl)$_2$] is a different species, it is still observed that both sulfonates chelated the cobalt center.

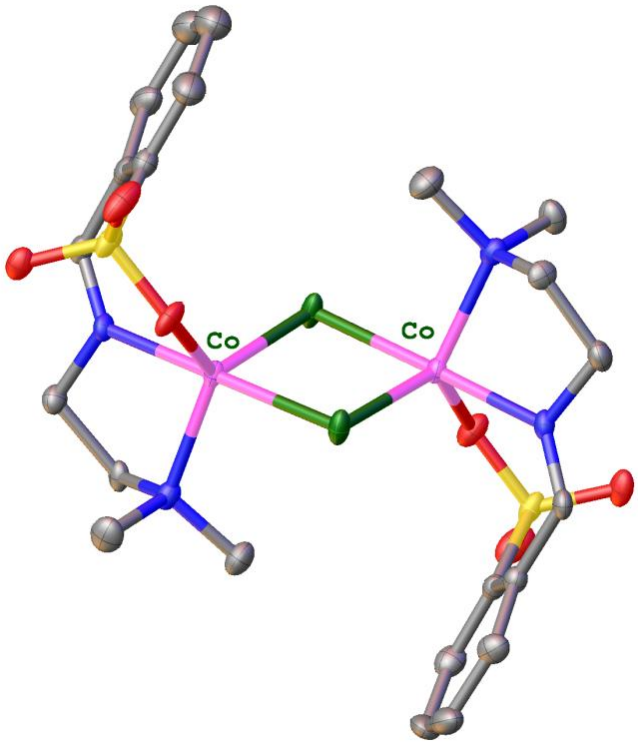

Figure 17. X-ray crystal structure of [(**13**)$_2$Co$^{II}_2$(μ-Cl)$_2$]. Hydrogens are omitted for clarity.

Even if the sulfonates are coordinating to the metal center, they are generally expected to be easily displaced by stronger donors, especially once the complex is electrochemically oxidized.

2.4 Preliminary Studies of Metal Complexes

Cyclic voltammetry was used to probe the electrochemical properties of the M(**13**)$_2$ (M = Mn^{II}, Fe^{II}) and [(**13**)$_2$Co$^{II}_2$(μ-Cl)$_2$] complexes in acetonitrile and dichloromethane. If the sulfonates do convert the imines to amidos, an irreversible redox

event should be observed, because the amidos should stabilize higher metal oxidation states, therefore making the reduction of the metal center more difficult. However, if a reversible redox event is observed, then it is possible the metal oxidation induced ring-chain isomerism cannot be observed on the cyclic voltammetry time scale.

In Figure 18, the cyclic voltammogram (CV) of $[(\mathbf{13})_2Co^{II}{}_2(\mu\text{-}Cl)_2]$ reveals two oxidation waves (-0.163, -0.561 V) and two reduction waves (-0.246, -2.000 V). The appearance of the irreversible redox event arises from mixed-valency, suggesting $[(\mathbf{13})_2Co^{II}{}_2(\mu\text{-}Cl)_2]$ behaves like a Class I mixed valence compound.[55] A reversible redox event is observed in the CV of $Mn(\mathbf{13})_2$ (-0.079 , -0.195 V, Figure 18).

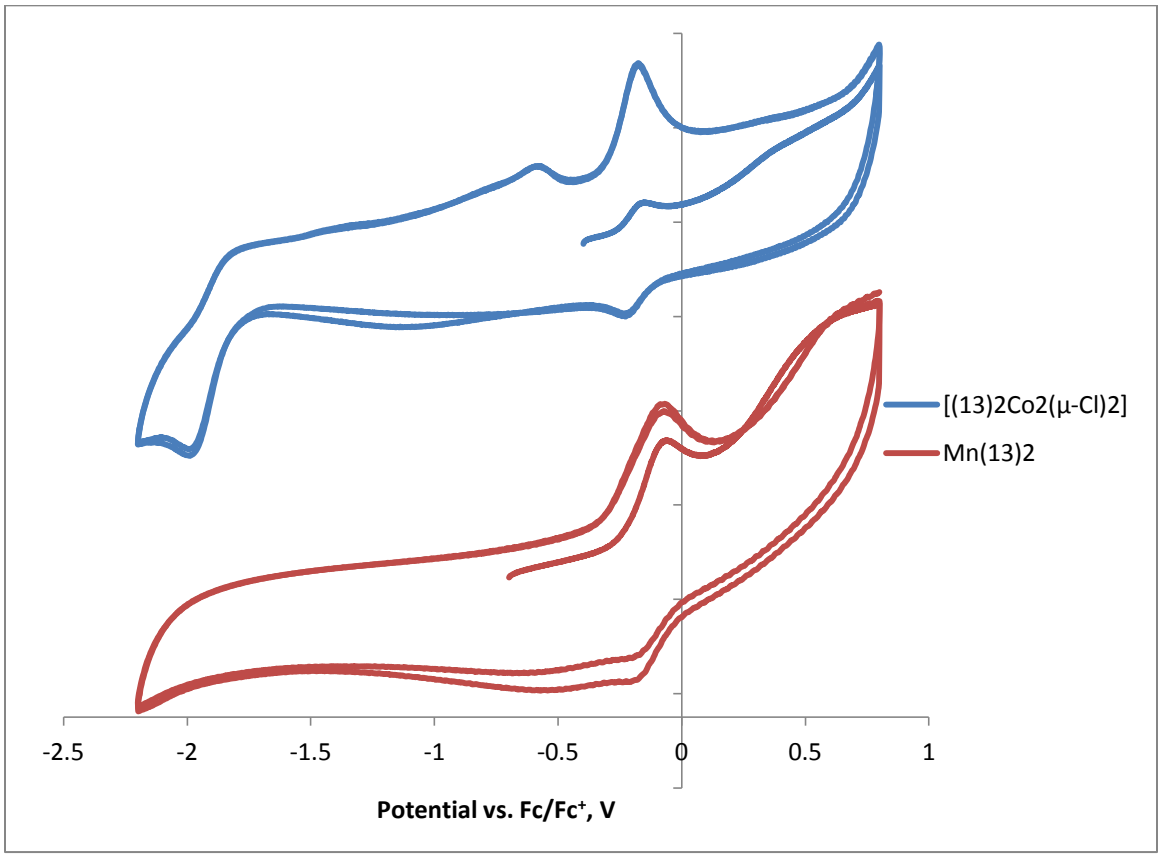

Figure 18. CVs of the manganese and cobalt complexes in acetonitrile with **13** ligands with a scanning rate of 0.1 V/s.

Unfortunately, both Mn(**13**)$_2$ and [(**13**)$_2$Co$^{II}_2$(μ-Cl)$_2$] CVs consist of reversible redox events, which are inconclusive for oxidation induced ring-chain isomerism. In contrast, the Fe(**13**)$_2$ CV only has an oxidation event at 345 mV, suggesting the possibility of oxidation induced ring-chain isomerism (Figure 19).

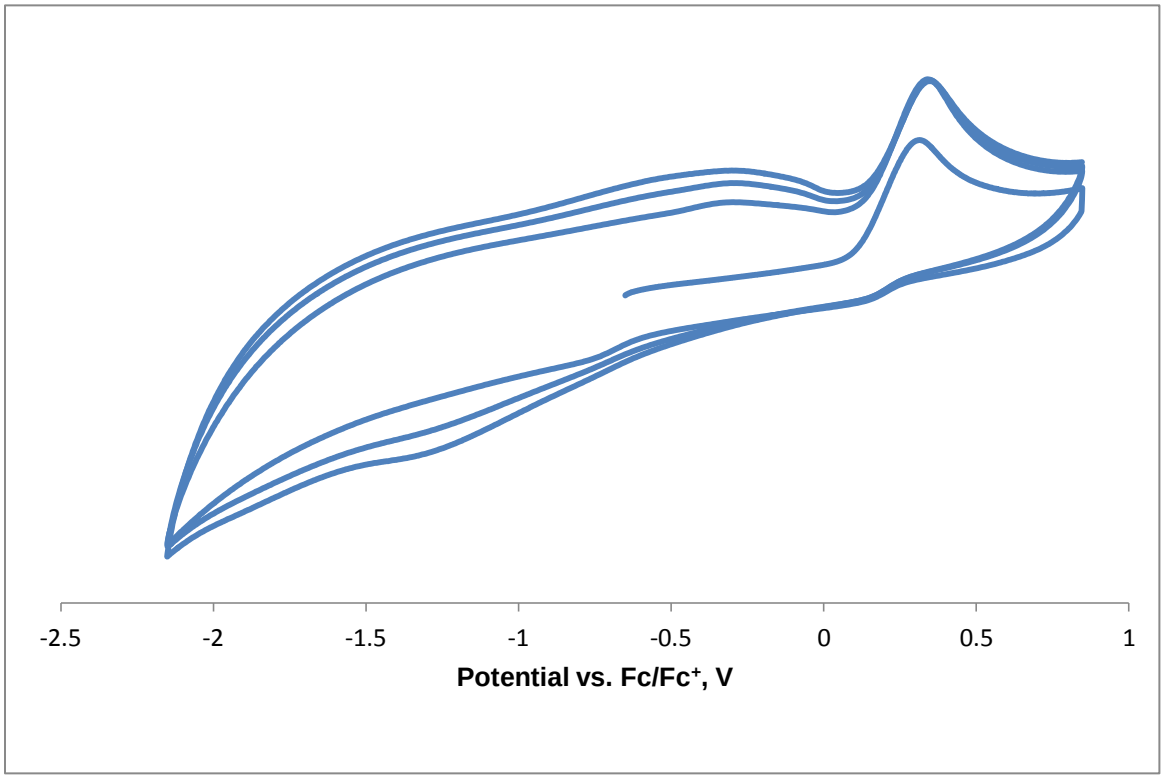

Figure 19. CV of Fe(**13**)$_2$ in acetonitrile showing only an oxidation wave with a scanning rate of 0.1 V/s.

The CV of Fe(**13**)$_2$ reveals that acetonitrile could be displacing the sulfonates to result in this electrochemical irreversibility. Specifically, the data suggests that once Fe(**13**)$_2$ have had its sulfonate oxygens displaced by solvent-derived acetonitrile ligands followed by an electrochemical one-electron oxidation, the sulfonates are able to convert the imine to the amido chelate, resulting in an irreversible redox event observed at 345 mV (Scheme 13). This proposal can account for the electrochemical irreversibility of the oxidation event for Fe(**13**)$_2$ in acetonitrile.

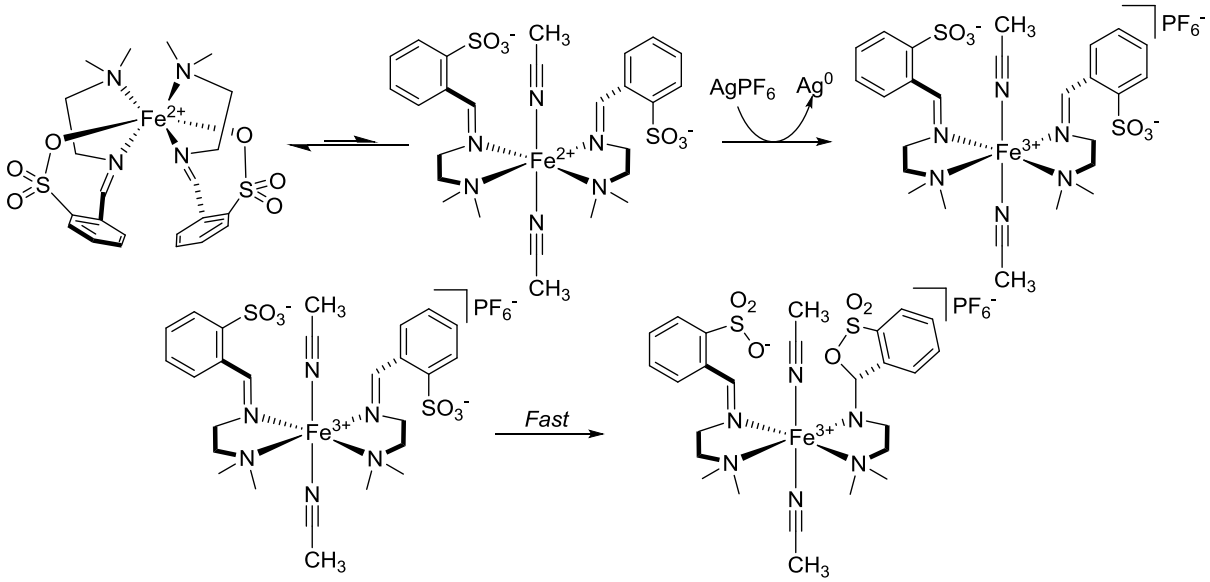

Scheme 13. Proposed reaction of Fe(**13**)$_2$ and $AgPF_6$ in acetonitrile.

When the Fe(**13**)$_2$ complex is placed in dichloromethane instead of acetonitrile, a reversible redox event is observed in the CV (472 mV and 332 mV, Figure 20B).

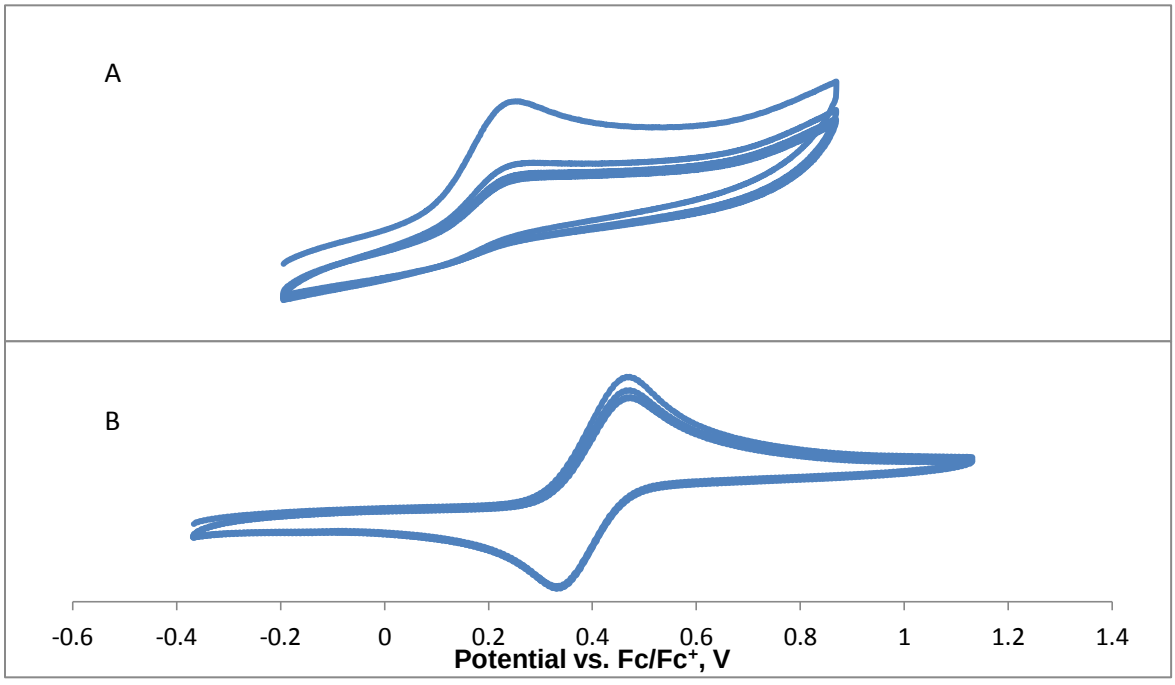

Figure 20. A) Close up of the CV for Fe(**13**)$_2$ in acetonitrile B) Close up of the CV for Fe(**13**)$_2$ in dichloromethane. Both CVs were done with a scanning rate of 0.1 V/s.

The CV of Fe(**13**)$_2$ in dichloromethane suggests that without a coordinating solvent, the sulfonate ligands are not displaced, ruling out oxidation-induced ring-chain isomerism.

With the promising CVs of the Fe(**13**)$_2$ complex in acetonitrile and dichloromethane, Fe(**13**)$_2$ was subjected to O_2 uptake studies. The Fe(**13**)$_2$ complex was dissolved in acetonitrile and was stirred under an O_2 atmosphere for 14 hours. O_2 consumption was measured by the volume of mineral oil that entered the Dean-Stark trap of the O_2 uptake apparatus (Figure S1). Over a 14-hour period, the Fe(**13**)$_2$ solution under an O_2 atmosphere underwent a color change from bright yellow to a dull orange, indicating Fe(**13**)$_2$ had undergone a chemical change, potentially forming an Fe-O_2 species. Unfortunately, the zwitterionic ligand **13** was the only isolable product obtained as crystalline material (see Appendix). In addition, the O_2 uptake experiment of Fe(**13**)$_2$ was repeated and inconsistent results were found (Figure S2 and S3).

Although O_2 uptake experiments yielded inconsistent results, both experiments suggested that Fe(**13**)$_2$ complex was consuming O_2. However, the O_2 uptake experiments must be repeated to determine what happens to Fe(**13**)$_2$ and how much O_2 is actually consumed.

From the CV data of Fe(**13**)$_2$, it is shown that coordinating solvents have a significant coordination effect on the complex. Fe(**13**)$_2$ CV data suggests that in order to induce ring-chain isomerism, ligands need to be added to displace the sulfonates to allow for the conversion of imines into amidos for the stabilization of higher oxidation states of Fe. Namely, strong σ-donors and π-acceptors are necessary to displace the sulfonates.

Introduction of π-acceptor ligands could also have the potential of inducing ring-chain isomerism by backbonding to the metal center making it more electron-deficient. With a more electron-deficient metal center, we can envision the displaced sulfonates being able to convert the imines into amido chelates to aid in stabilizing the metal center.

Once the sulfonates have been displaced by other ligands, oxidation studies can be performed on the Fe^{II} complex with free sulfonates. Ideally, what should be observed for the oxidation studies would be the cyclization of the free sulfonates onto the imines to afford the amido ligation. The results of the oxidation studies will guide new designs for these ERLs that can be used in catalysis.

3.0 Conclusion

After exploring various synthetic routes, we identified a rational synthesis that can afford **11d**, the precursor to ERL **1**. This 4-step synthesis can generate various derivatives of ERLs via **10** where the aryl imine and pendant nucleophile can be altered to garner **2** and **3** (Scheme 14).

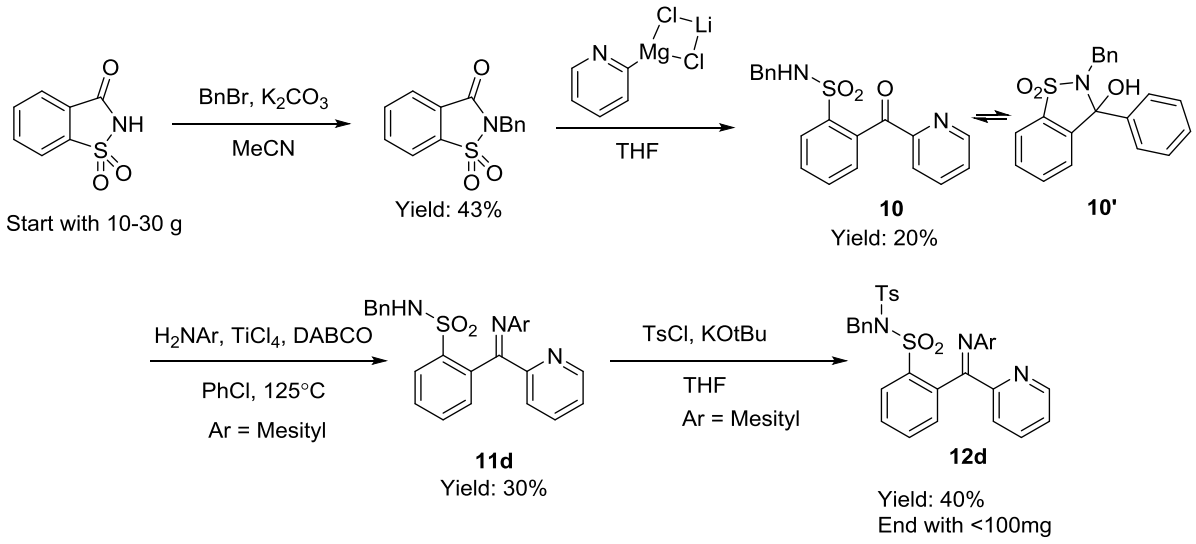

Scheme 14. Synthetic route to **12d**, precursor to ERL **1**.

Through this synthesis, compounds **11a-e** demonstrated that sterics play a critical role in affecting the ring-chain equilibrium for these systems. Additionally, **11d** was treated as a potential ligand and was metallated to an Fe^{II} center without success, possibly due to the benzyl sulfonamide being too nucleophilic for the ideal ERL.[56] In this study, compounds **10**, **11d**, **11e**, and **12d** are consistent with compounds that exhibit ring-chain isomerism, which reinforce the concept that ERLs should be able to alter coordination states in response to the changes in metal oxidation states once metallated.

Although this synthesis produced **12d**, only small quantities were obtained. The limitations of this ligand synthesis stems from the pyridyl addition and the amine condensation, where the highest reproducible yields obtained are 20% and 30%, respectively. There were attempts to optimize the pyridyl addition utilizing different types of organometallic reagents, however, the turbo Grignard proved to be the highest yielding in all cases, albeit 20% yield (see Appendix).

After realizing the initial ERL synthesis was not viable for producing sufficient material for subsequent studies of coordination complexes, modified ligand platforms were designed, where the sulfonimidate was replaced by a sulfonate (Figure 21).

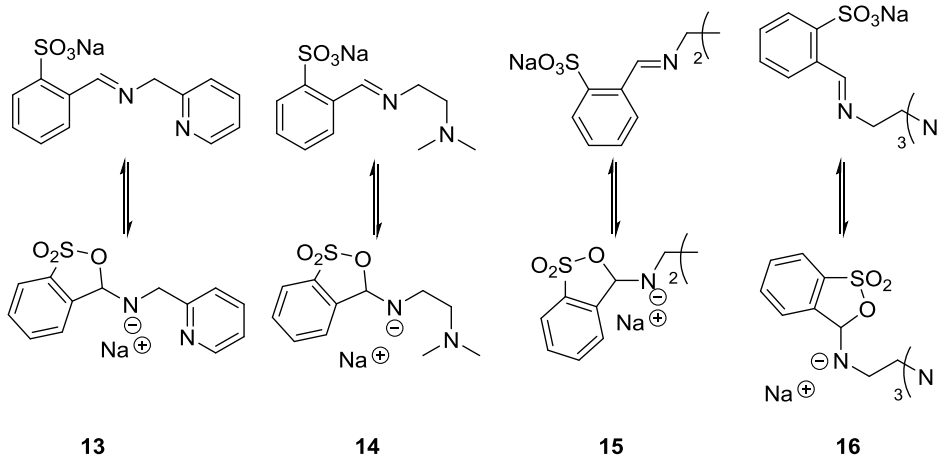

Figure 21. Alternative ERL platforms with chain and ring forms.

We were able to use **13** to address how this alternative ERL would chelate to the metal center. Crystal structures of the M(**13**)$_2$ reveal that the sulfonates, although weak ligands, can still coordinate to the metal center and, in general, they can do so even in the presence of coordinating solvents. Since the sulfonates are able to bind to the metal center, it is possible that increasing the sterics to the pendant nucleophile could reduce the potential of binding to the metal center for these ligands. An alternative method was to displace the sulfonate ligands with π-acceptor ligands, such as cyanide, 2,2'-bipyridine (bpy), or acetonitrile. By introducing π-acceptor ligands, it is predicted that when they backbond to the metal center, it could potentially induce ring-chain isomerism in **13**.

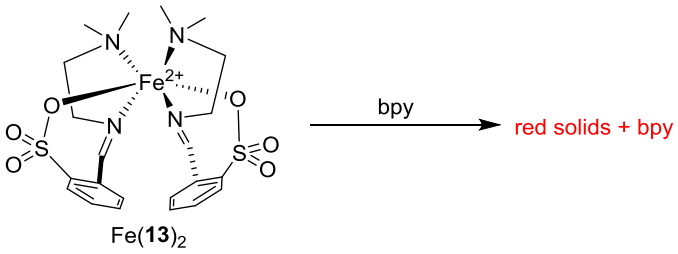

Scheme 15. Attempted bpy ligation of Fe(**13**)$_2$.

Efforts towards mono-ligation of bpy to Fe(**13**)$_2$ resulted in soluble red solids found only to contain bpy (Scheme 15). In addition, there were intractable deep red solids that were slightly soluble in DMF and could not be unambiguously identified.

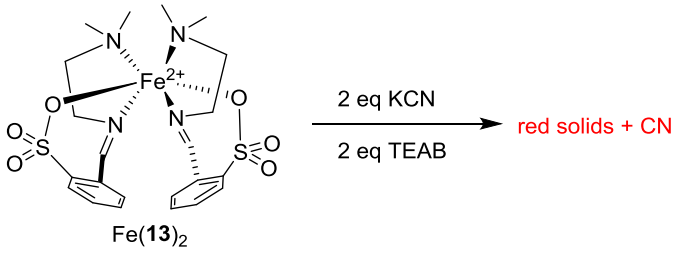

Scheme 16. Attempted cyanide ligation of Fe(**13**)$_2$.

Cyanide binding onto the Fe(**13**)$_2$ was attempted and red solids were obtained, but the solids were only slightly soluble in DMF (Scheme 16). Infrared spectroscopic

analysis of the crude residue confirmed the presence of cyanide. However, similar to the attempt at mono-ligation of bpy to Fe(**13**)$_2$, the red solids could not be unambiguously identified.

Due to the difficulties in obtaining the Fe(**13**)$_2$ octahedral complex with free sulfonates, an alternative route to this species is proposed in Scheme 17.

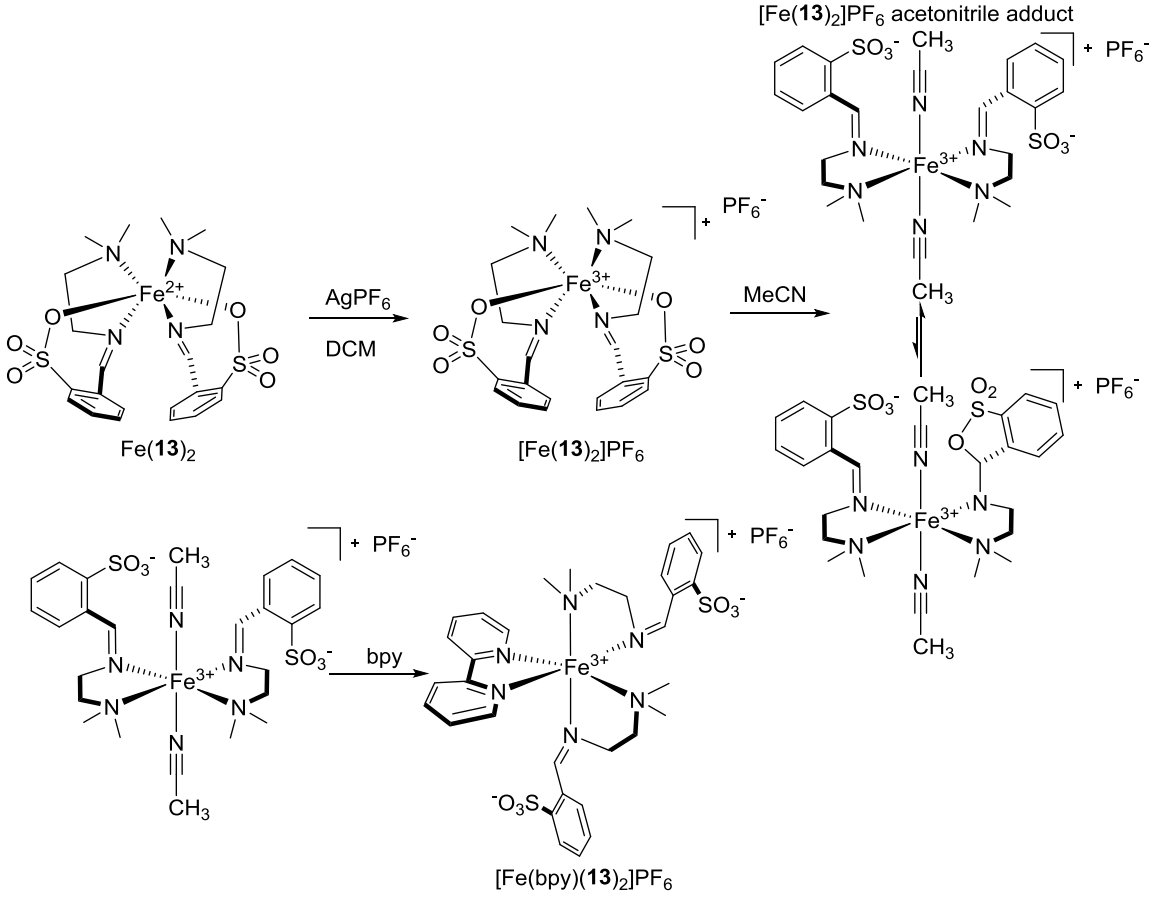

Scheme 17. Proposed synthesis for [Fe(bpy)(**13**)$_2$]PF$_6$.

Based on the Fe(**13**)$_2$ CV data, a one-electron oxidation of the Fe(**13**)$_2$ to generate [Fe(**13**)$_2$]PF$_6$ could allow for the potential displacement of the sulfonates and access to the [Fe(**13**)$_2$]PF$_6$ acetonitrile adduct (Scheme 17). With the [Fe(**13**)$_2$]PF$_6$ acetonitrile adduct, a π-acceptor, like bpy, could be used to generate the [Fe(bpy)(**13**)$_2$]PF$_6$. Once

[Fe(bpy)(**13**)$_2$]PF_6 is isolated and fully characterized, oxidation studies could afford a high valent Fe^{IV} center with the ring form(s) of **13**.

4.0 Future Studies

The immediate work will be to synthesize and fully characterize the [Fe(**13**)$_2$]PF_6 and determine if the acetonitrile ligands are capable of displacing the sulfonates. Furthermore, attempts to ligate other π-acceptor ligands onto [Fe(**13**)$_2$]PF_6 can address if the sulfonates could be displaced to obtain the desired octahedral Fe^{III} complexes. If successful, the octahedral Fe^{III} complexes could be examined for their redox properties using cyclic voltmmatetry. Once the redox potential is established and shown to be feasible, a one-electron oxidation could garner access to the high valent Fe^{IV} center. Ideally, if the Fe^{IV} center is accessible, the complex will need to be isolated and fully characterized to determine if the sulfonates have converted the imines into amidos to stabilize the high valent Fe^{IV} center.

If the Fe^{IV} center is not accessible or obtainable, different metal centers (potential alternative metal centers: Mn^{II}, Cr^{II}) could be used. The alternative metal centers mentioned are capable of accessing multiple oxidation states that would allow for studies to be done on the metal oxidation induced ring-chain isomerism. Chromium would be a particularly good metal for this study as multiple oxidations states, ranging from +2 to +6 (e.g. $CrCl_2$ and Jones Reagent), could be accessed.

Once a complex with the cyclic form(s) of **13** is obtained, the next step would be to determine the rules for the metal-oxidation induced ring-chain isomerism. In this study, multiple ligands with different pendant nucleophiles are required. With the various pendant nucleophiles, oxidation studies could show how the pendant nucleophiles will

respond to the change in metal oxidation states. In this respect, my work will help guide future designs of ERLs with potential applications in catalysis.

5.0 Supporting Information

General Considerations.

Glassware was oven-dried >100°C before use. All reactions were performed under an inert atmosphere (nitrogen) unless noted otherwise. All commercially available chemicals were purchased from the following sources: Sigma Aldrich, TCI America, Alfa Aesar, Strem Chemicals, and Fisher Scientific. All commercially available chemicals were used without purification unless noted. The organometallic reagents were synthesized in flame dried glassware under an inert atmosphere. All dry solvents were obtained from the SPS system.

Column chromatography was performed in silica gel with the Biotage Isolera Spektra One and Four.

All proton and carbon NMR spectra were recorded on the following instruments – Varian INOVA 400MHz NMR and Varian Mercury 300MHz. ^{1}H NMR data are reported as the following: parts per million (ppm), chloroform-*d* (δ = 7.27, unless noted otherwise), multiplicity (s = singlet, d = doublet, t = triplet, q = quartet, sp = septet, dd = doublet of doublets, ddt = doublet of doublet of triplets, td = triplet of doublets, ddd = doublet of doublet of doublets, m = multiplet, bs = broad singlet), coupling (Hz), and integration. Chemical shifts for ^{13}C NMR are described in parts per million from chloroform-*d* (δ = 77.23) unless noted otherwise. Mass spectra were taken on the JEOL JMS-SX102/SX102A/E mass spectrometer. IR spectra were collected through the Nicolet 380 FT-IR on an ATR plate.

1M 2-Bromopyridyl Grignard Reagent Preparation

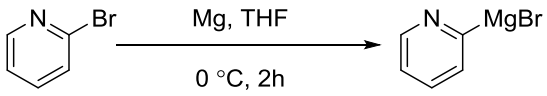

The Grignard procedure was adapted from Paquette and coworkers.[50] To a flame dried Schlenk flask, magnesium (111.8 mg, 4.6 mmol, 1 eq.) turnings was added and the flask was purged of air. THF (9.2 mL, 0.5 M) was added to the flask and cooled to 0 °C (CAUTION: Reaction will reflux). Once cooled to 0 °C, 2-bromopyridine (0.440 mL, 4.6 mmol, 1 eq.) was added to the solution and allowed to stir at 0 °C for 15 minutes and then allowed to stir to room temperature for 2 hours. The reaction mixture turned to a dark green solution (magnesium turnings may still be in solution).

1M 2-Bromopyridyl Turbo Grignard Reagent Preparation

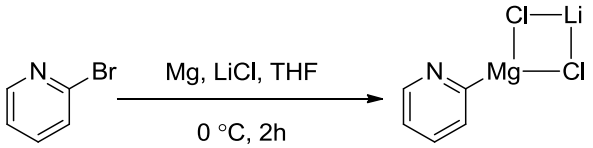

The turbo Grignard procedure was adapted from Knochel and coworkers.[51] To a flame dried Schlenk flask, magnesium turnings (509 mg, 21.2 mmol, 2.50 eq.) and lithium chloride (449 mg, 10.6 mmol, 1.25 eq.) were added and the flask was purged of air. To the flask, THF (9 mL, 1.0M) was added and cooled to 0 °C. Once cooled, 2-bromopyridine (808 µL, 8.5 mmol, 1.00 eq.) was added to the solution and allowed to stir at 0 °C for 15 minutes. The reaction was stirred at room temperature for 2 hours (CAUTION: Reaction might reflux). The reaction mixture turned a dark brown solution (magnesium turnings may still be in solution).

General Grignard/ Turbo Grignard Addition Reactions

The procedure was adapted from Paquette and coworkers.[50] The amide or ester was added to a flame dried 2-neck round bottom under nitrogen. The amide (1.0 eq.) was dissolved in THF (1.0M, unless noted otherwise). The 2-organometallic pyridyl 1.0M solution (1.1 eq.) was added to the solution of sulfonamide in THF slowly at room temperature and was stirred for 6 hours at room temperature. The reaction mixture was quenched with saturated ammonium chloride (10 mL / g of sulfonamide) and extracted with dichloromethane (10 mL / g of sulfonamide). The organic layer was dried with Na_2SO_4, filtered, and concentrated under reduced pressure. The crude product was purified through silica column chromatography or recrystallization.

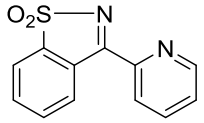

7

Synthesized from THF (10.65 mL), saccharin (1.95 g, 10.7 mmol), and turbo pyridyl Grignard solution (11.7 mL, 11.7 mmol). The crude product was dissolved in a minimum amount of hot EtOH. Once the solution was cooled, **7** was recrystallized as an amorphous brown solid (0.208 g, 8%).

^{1}H NMR (400 MHz, $CDCl_3$) δ 9.14 (ddd, *J* = 5.5, 2.4, 1.6 Hz, 1H), 8.87 (ddd, *J* = 4.8, 1.8, 0.9 Hz, 1H), 8.49 (dt, *J* = 8.0, 1.0 Hz, 1H), 8.07 – 7.85 (m, 2H), 7.86 – 7.70 (m, 2H), 7.60 (ddt, *J* = 7.7, 4.8, 1.0 Hz, 1H). ^{13}C NMR (400 MHz, $CDCl_3$) δ 167.5, 150.8, 149.8, 140.9, 137.5, 133.9, 133.3, 130.6, 130.6, 127.7, 126.2, 122.4. FTMS + c APCI $\{C_{12}H_8N_2O_2S\}^+$ [M+H] – calcd 245.0385, obsd 245.0378 (Δ=2.48)

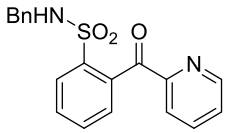

10

Synthesized from THF (15 mL), benzyl saccharin (4.0 g, 14.6 mmol), and turbo pyridyl Grignard (16.1 mL, 16.1 mmol). The crude product was purified by flash chromatography with hexanes:EtOAc (1:1, v:v) eluent to obtain **10** as a yellow oil (1.03 g, 20%). **Note**: There were two isomers observed in equilibrium in solution when characterized.

^{1}H NMR (400 MHz, $CDCl_3$) δ 8.50 (d, *J* = 4 Hz, 1H), 8.19 (d, *J* = 8 Hz, 1H), 7.99 (d, *J* = 8 Hz, 1H), 7.87 (m, 1H), 7.66-7.38 (m, 5H), 7.19-7.02 (m, 5H), 5.87 (t, 1H), 4.24 (d, *J* = 8Hz, 2H). ^{13}C NMR (400 MHz, $CDCl_3$, **10** and **10'**) δ 196.3, 155.5, 152.9, 148.9, 146.4, 140.2, 137.9, 137.8, 137.6, 137.3, 137.2, 135.8, 133.9, 133.6, 131.8, 130.6, 130.0, 129.7, 128.8, 128.6, 128.5, 127.9, 127.8, 127.7, 127.5, 127.0, 124.6, 124.2, 124.0, 122.2, 87.9, 47.6, 41.9. FTMS + c ESI $\{C_{19}H_{16}N_2O_3S\}^+$ [M+H] – calcd 353.0955, obsd 353.0957 (Δ=0.45)

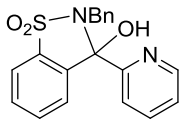

10'

In equilibrium in solution with **10**, with a ratio of 1 : 0.76 chain : ring (**10** : **10'**).

^{1}H NMR (400 MHz, $CDCl_3$) δ 8.43 (d, *J* = 4 Hz, 1:0.76, 1H), 7.87 (m, 1H), 7.65-7.37 (m, 5H), 7.28 (s, 6H), 4.48 (d, *J* = 20 Hz, 1H), 4.29 (d, *J* = 20 Hz, 1H).

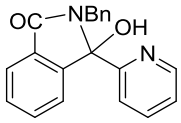

10"

Synthesized from THF (4.2 mL), benzyl phthalimide (1.0 g, 4.2 mmol), and pyridyl Grignard solution (4.6 mL, 4.6 mmol). The crude solids were dissolved in a minimum amount of EtOAc. The crude product was purified by flash chromatography with hexanes:EtOAc (1:1, v:v) eluent to obtain **10''** as a white solid (266 mg, 20%).

^{1}H NMR (400 MHz, $CDCl_3$) δ 8.72 (d, *J* = 4 Hz, 1H), 8.13 (d, *J* = 8 Hz, 1H), 7.72 (t, *J* = 4Hz, 2H), 7.44 (m, 5H), 7.29 (m, 2H), 7.25 (m, 1H), 4.89 (d, *J* = 20 Hz, 1H), 4.57 (d, *J* = 20 Hz, 1H).

Benzylation Synthesis

The procedure for preparing benzylated saccharin and phthalimide was adapted from Lehn and coworkers.[57] To a round bottom, MeCN (0.25M) was added an amine (1.0 eq.) and K_2CO_3 (1.3 eq.). The reaction mixture was stirred for 5 minutes and benzyl bromide (1.2 eq.) was added to the mixture. The reaction mixture was refluxed for 24 hours and was concentrated. After concentration, the reaction was redissolved in DCM (0.50M), filtered to remove K_2CO_3, and concentrated under reduced pressure. The crude product was recrystallized from a minimum amount of hot ethanol. Once the solution had cooled, the desired product was collected through filtration.

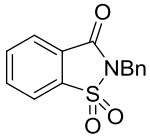

Synthesized from MeCN (153 mL), saccharin (7.0 g, 38.3 mmol), K_2CO_3 (6.9 g, 49.8 mmol), and benzyl bromide (5.4 mL, 45.9 mmol). The product was isolated as a white amorphous solid (16.0 g, 71%).

^{1}H NMR (400 MHz, $CDCl_3$) δ 8.40 (d, *J* = 8Hz, 1H), 7.92 (d, *J* = 4 Hz, 1H), 7.83 (m, 2H), 7.49 (d, *J* = 4 Hz, 2H), 7.33 (m, 3H), 4.89 (s, 2H). ^{13}C NMR (400 MHz, $CDCl_3$) δ 159.1, 137.9, 135.0, 134.7, 134.6, 128.9, 128.9, 128.5, 127.5, 125.5, 121.3, 42.9. FTMS + c APCI $\{C_{14}H_{12}NO_3S\}^+$ [M+H] – calcd 274.05324, obsd 274.05333 (Δ=0.33)

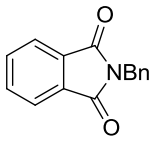

Synthesized from MeCN (125 mL), phthalimide (9.3 g, 50.2 mmol), K_2CO_3 (9.0 g, 65.3 mmol), and benzyl bromide (10.3 g, 60.2 mmol). The product was isolated as a white amorphous solid (5.0 g, 42%).

^{1}H NMR (400 MHz, $CDCl_3$) δ 7.85 (q, *J* = 4 Hz, 2H), 7.72 (q, *J* = 4 Hz, 2H), 7.44 (m, 2H), 7.31 (m, 3H), 4.86 (s, 2H).

$TiCl_4$ promoted Imine Formation Procedure

The procedure to generate aminal was taken from Yamamoto and coworkers.[53] To a 50mL round bottom flask, **10** (1.0 eq.), 1,4-diazabicyclo[2.2.2]octane (DABCO) (6.0 eq.), and aryl amine (2.5 eq.) were dissolved in chlorobenzene (0.10M). To the mixture, $TiCl_4$ (1.5 eq.)was added and the reaction mixture was stirred at 125 °C under nitrogen for 15 hours. The precipitate was filtered through celite and washed with EtOAc (10 mL /

g of **10**). The filtrate was concentrated under reduced pressure. The crude residue was purified by flash chromatography with hexanes:EtOAc eluent.

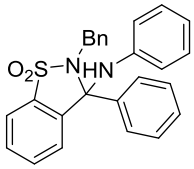

11a

Synthesized from chlorobenzene (15 mL), **10** (527 mg, 1.50 mmol), DABCO (1.00 g, 8.97 mmol), aniline (341 μL, 3.74 mmol), and $TiCl_4$ (160 μL, 2.24 mmol). The crude product was purified by flash chromatography with hexanes:EtOAc (4:1→1:1, v:v) eluent gradient and obtained **11a** as a tan solid (220 mg, 34%).

^{1}H NMR (400 MHz, $CDCl_3$) δ 8.47 (ddd, *J* = 4.9, 1.8, 0.9 Hz, 1H), 7.99 (dt, *J* = 7.9, 0.8 Hz, 1H), 7.55 (td, *J* = 7.6, 1.0 Hz, 1H), 7.51 – 7.37 (m, 3H), 7.31 – 7.23 (m, 1H), 7.22 – 7.03 (m, 7H), 6.81 – 6.67 (m, 2H), 6.62 (dt, *J* = 7.8, 1.1 Hz, 3H), 4.38 (d, *J* = 15.4 Hz, 1H), 4.27 (d, *J* = 15.4 Hz, 1H). ^{13}C NMR (400 MHz, $CDCl_3$) δ 157.2, 147.1, 142.7, 140.0, 137.7, 135.6, 135.5, 133.8, 130.5, 129.4, 129.3, 128.0, 127.3, 124.6, 123.6, 122.7, 121.5, 119.4, 115.8, 80.4, 42.9. IR (neat) cm^{-1} 3329, 3055, 2918, 1600, 1502, 1469, 1453, 1431, 1365, 1288, 1225, 1208, 1170, 1156, 1131, 1096, 1079, 1049, 1026, 996, 913, 844, 743, 6923, 654, 621, 597, 568, 538.

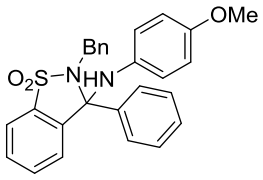

11b

Synthesized from chlorobenzene (13 mL), **10** (461 mg, 1.30 mmol), DABCO (880 mg, 7.85 mmol), *p*-anisidine (402 mg, 3.74 mmol) and $TiCl_4$ (215 μL, 1.96 mmol). The crude

product was purified by flash chromatography with hexanes:EtOAc (2:1, v:v) eluent and obtained **11b** as an orange red solid (148 mg, 25%).

^{1}H NMR (300 MHz, $CDCl_3$) δ 8.54 – 8.36 (m, 1H), 7.96 (dd, *J* = 7.9, 0.9 Hz, 1H), 7.52-7.42 (m, 3H), 7.26 – 7.20 (m, 9H), 6.69 – 6.49 (m, 4H), 4.41(d, *J* = 15.3 Hz, 1H), 4.28 (d, *J* = 15.3 Hz, 1H), 3.68 (s, 3H).

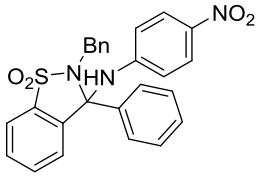

11c

Synthesized from chlorobenzene (38 mL), **10** (1.35 g, 3.80 mmol), DABCO (2.55 g, 22.8 mmol), *p*-nitroaniline (1.31 g, 9.50 mmol) and $TiCl_4$ (0.624 mL, 5.70 mmol). The crude product was purified by flash chromatography with hexanes:EtOAc (2:1, v:v) eluent and obtained **11c** as a red solid (27 mg, 2.0%).

^{1}H NMR (300 MHz, $CDCl_3$) δ 8.58 (d, *J* = 3.0 Hz, 1H), 8.06 (d, *J* = 3 Hz, 1H), 7.90 (d, *J* = 6.0 Hz, 2H), 7.67 – 7.62 (m, 2H), 7.61 – 7.50 (m, 1H), 7.32 (d, *J* = 6.0 Hz, 1H), 7.14 (d, *J* = 6.0 Hz, 1H), 7.08-6.99 (m, 4H), 6.45 (d, *J* = 6.0 Hz, 2H), 4.35 (d, *J* = 18.0 Hz, 1H), 3.96 (d, *J* = 18.0 Hz, 1H).

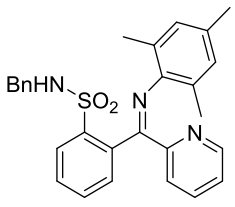

11d

Synthesized from chlorobenzene (12.6 mL), **10** (444 mg, 1.26 mmol), DABCO (849 mg, 7.52 mmol), 2,4,6-trimethylaniline (443 μL, 3.15 mmol) and $TiCl_4$ (207 μL, 1.89 mmol). The crude product was purified by flash chromatography with hexanes:EtOAc (2:1, v:v)

eluent and obtained **11d** as a yellow solid (148 mg, 25%). **Note**: There were two isomers observed in equilibrium in solution when characterized.

^{1}H NMR (600 MHz, $CDCl_3$) δ 8.40 (d, *J* = 4.8 Hz, 0.3H), 8.06 (d, *J* = 7.2 Hz, 1H), 8.04 (d, *J* = 4.8 Hz, 1H), 7.92 (d, *J* = 8.4 Hz, 1H), 7.86 (m, 1H), 7.60 – 7.42 (m, 3H), 7.26 – 6.96 (m, 5H), 6.71 (s, 2H), 4.01 (d, *J* = 6 Hz, 2H), 2.20 (s, 3H), 2.01 (s, 6H). ^{13}C NMR (600 MHz, $CDCl_3$, **11d** and **11d**') δ 166.9, 154.7, 149.3, 147.6, 147.6, 147.6, 144.4, 138.8, 137.9, 137.6, 137.4, 135.9, 135.0, 133.4, 132.9, 132.6, 132.3, 132.1, 130.6, 129.4, 128.9, 128.9, 128.6, 128.1, 128.0, 127.8, 126.6, 125.3, 124.5, 124.1, 123.0, 105.9, 82.1, 48.0, 47.9, 21.3, 20.9, 20.8, 18.5, 14.4. FTMS + c APCI $\{C_{28}H_{28}N_3O_2S\}^+$ [M+H] – calcd 470.1896, obsd 470.1896 (Δ=1.70)

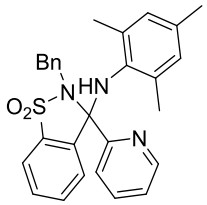

11d'

In equilibrium in solution with **11d**, with a ratio of 1 : 0.6 chain : ring (**11d** : **11d'**).

^{1}H NMR (600 MHz, $CDCl_3$) δ 8.58 (d, *J* = 7.2 Hz, 1H), 8.04 (d, *J* = 4.8 Hz, 1H), 7.92 (d, *J* = 8.4 Hz, 1H), 7.86 (m, 1H), 7.60 – 7.42 (m, 4H), 7.35 (m, 2H), 7.26 – 6.96 (m, 5H), 4.36(dd, *J* = 13.2, 8.4 Hz, 1H), 3.98 (dd, *J* = 9.6, 4.2 Hz, 1H), 2.20 (s, 3H), 2.01 (s, 6H).

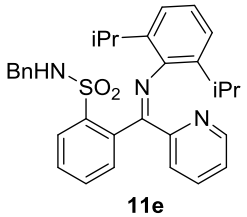

11e

Synthesized from chlorobenzene (12.6 mL), **10** (1.00 g, 2.8 mmol), DABCO (1.88 g, 16.8 mmol), 2,6-diisopropylaniline (1.32 mL, 7.0 mmol) and $TiCl_4$ (0.46 mL, 4.2 mmol). The

crude product was purified by flash chromatography with hexanes:EtOAc (2:1, v:v) eluent and obtained **11e** as a brown solid (0.54 g, 37%). **Note**: There were two isomers observed in equilibrium in solution when characterized.

^{1}H NMR (300 MHz, $CDCl_3$) δ 9.14 – 9.13 (dd, *J* = 6, 3 Hz, 1H), 8.49 (d, *J* = 6Hz, 1H) 7.98 (m, 1H), 7.60 – 7.49 (m, 4H), 7.10 (s, 3H), 7.26 – 7.20 (m, 4H), 6.69 – 6.49 (m, 2H), 4.12 (d, *J* = 6 Hz, 2H), 1.13 (d, *J* = 6 Hz, 3H). 1.08 (d, *J* =6 Hz, 6H).

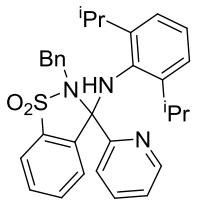

11e'

In equilibrium in solution with **11e**, with a ratio of 1 : 0.3 chain : ring (**11e** : **11e'**).

^{1}H NMR (300 MHz, $CDCl_3$) δ 8.88 (d, *J* = 1 Hz, 1H), 8.49 (d, *J* = 6Hz, 1H) 7.98 (m, 1H), 7.60 – 7.49 (m, 4H), 7.26 – 7.20 (m, 4H), 6.69 – 6.49 (m, 4H), 4.60 (d, *J* = 13.0 Hz, 1H), 4.36 (d, *J* = 12.0 Hz, 1H), 1.13 (d, *J* = 6 Hz, 3H). 1.08 (d, *J* =6 Hz, 6H).

Tosylation of Benzyl Sulfonamide 12d

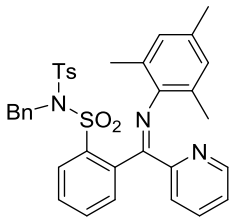

12d

To a 20 mL scintillation vial, KO^{t}Bu (53 mg, 0.55 mmol, 1.1 eq.) was added to a solution of **11d** (250 mg, 0.504 mmol, 1.0 eq.) in THF (2 mL, 0.28 M). The solution was stirred for 5 minutes at room temperature and then TsCl (134 mg, 0.605 mmol, 1.2 eq.) was added to the mixture. Then, the reaction mixture was stirred for 12 hours. KCl was filtered out and the crude product was concentrated under reduced pressure. The crude

product was purified by flash chromatography with hexanes:EtOAc (1:1, v:v) eluent and obtained **12d** as a yellow solid in (107 mg, 33%). **Note**: There were two isomers observed in equilibrium in solution when characterized.

^{1}H NMR δ (400 MHz, $CDCl_3$) 8.39 (d, *J* = 4.8 Hz, 1H), 8.22 (d, *J* = 8 Hz, 1H), 8.35 (d, *J* = 4.0 Hz, 1H), 7.88 (d, *J* = 8.8 Hz, 1H), 7.78 (m, 2H), 7.63 (dd, *J* = 7.2 Hz, 1H), 7.51 (m, 1H), 7.32 (m, 3H), 7.19 (m, 8H), 7.01 (m, 6H), 6.76 (s, 2H), 4.77 (d, *J* = 16.0 Hz, 1H), 4.56 (s, 2H), 4.49 (d, *J* = 16.0 Hz, 1H), 2.34 (s, 3H), 2.24 (s, 3H), 2.05 (s, 3H), 2.02 (s, 6H). ^{13}C NMR (400 MHz, $CDCl_3$, **12d** and **12d'**) δ 168.1, 153.4, 148.5, 138.3, 136.9, 135.6, 134.9, 133.4, 133.3, 132.2, 129.8, 1291, 128.9, 128.8, 128.2, 128.1, 127.9, 126.1, 125.5, 124.5, 52.2, 44.7, 20.3, 19.6, 17.4, 17.2. FTMS + c APCI $\{C_{35}H_{33}N_3O_4S_2\}^+$ [M+H] – calcd 624.1991, obsd 624.1970 (Δ=3.36)

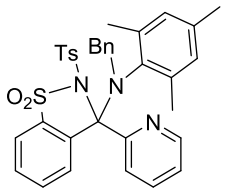

12d'

In equilibrium in solution with **12d**, with a ratio of 1 : 0.2 chain : ring (**12d** : **12d'**).

^{1}H NMR δ (400 MHz, $CDCl_3$) 8.39 (d, *J* = 4.8 Hz, 1H), 8.22 (d, *J* = 8 Hz, 1H), 8.35 (d, *J* = 4.0 Hz, 1H), 7.88 (d, *J* = 8.8 Hz, 1H), 7.78 (m, 2H), 7.63 (dd, *J* = 7.2 Hz, 1H), 7.51 (m, 1H), 7.32 (m, 3H), 7.19 (m, 8H), 7.01 (m, 6H), 6.76 (s, 2H), 4.77 (d, *J* = 16.0 Hz, 1H), 4.56 (s, 2H), 4.49 (d, *J* = 16.0 Hz, 1H), 2.32 (s, 3H), 2.15 (s, 3H), 2.06 (s, 6H).

Failed Transimination Procedures

***In situ* Lithio-isopropyl Amide Transimination Reaction**

To a 5mL round bottom flask, isopropylamine (40 µL, 0.467 mmol, 1.1 eq.) was dissolved in THF (1 mL, 0.5 M) and cooled to -78 °C. To the reaction mixture, 2.5 M nBuLi (20 µL, 0.514 mmol, 1.1 eq.) in hexanes was added. After 2 hours of stirring at -78 °C, a solution of **7** (100 mg, 0.425 mmol, 1.0 eq.) in THF (1 mL, 0.5 M) was added to the mixture and stirred at room temperature for 10 hours. The reaction was quenched with water and extracted with Et_2O (5 mL / g of **7**). The organic layer was dried with Na_2SO_4. The Na_2SO_4 was filtered and the crude mixture was concentrated under reduced pressure.

Neat Isopropylamine reaction

To a flame dried 15 mL sealed tube, **7** (100 mg, 0.425 mmol, 1 eq.) was dissolved in isopropylamine (3 mL, 0.14 M) and heated to 100 °C over 10 hours. The crude mixture was concentrated under reduced pressure to remove the isopropylamine.

Zinc-promoted Imine Formation

The procedure was adapted from Filgueiras and coworkers.[58] To flame dried 25 mL round bottom flask, **7** (100 mg, 0.425 mmol, 1 eq.), and isopropylamine (40 µL, 0.467 mmol, 1.1 eq.) were dissolved in methanol (3 mL, 0.1 M) and 1 drop of glacial acetic acid and the mixture was refluxed for 1.5 hours. After 1.5 hours, the reaction was cooled to room temperature and $ZnCl_2$ (57.9 mg, 0.425 mmol, 1 eq.) was added to the mixture and refluxed for another 2 hours. The reaction mixture was then cooled and the crude mixture was concentrated under reduced pressure.

$TiCl_4$-promoted Transimination

To a flame dried 5 mL round bottom flask, **7** (100 mg, 0.425 mmol, 1 eq.) and isopropylamine (40 µL, 0.467 mmol, 1.1 eq.) were dissolved in THF (1 mL, 0.5 M). To

the reaction mixture, $TiCl_4$ (70 µL, 0.638 mmol, 1.5 eq.) was added and stirred at room temperature for 5 hours. The mixture was then filtered through celite and the solvent was removed.

General Preparation of Ligands 13, 15, 16

A mixture of 2-formylbenzenesulfonic acid sodium salt and amine was refluxed in ethanol (0.5 M) with a Dean-Stark trap for 12 hours at 100 °C. The reaction was cooled to room temperature and the ethanol was removed under reduced pressure. Then, the solids were washed with chloroform (3 mL / g of 2-formylbenzenesulfonic acid sodium salt) and the product was filtered out without further purification.

13

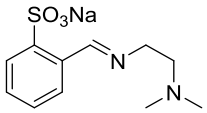

Synthesized from ethanol (48 mL), 2-formylbenzenesulfonic acid sodium salt (5.00 g, 24.06 mmol, 1.0 eq.) and N,N-dimethylethylenediamine (2.63 mL, 24.06 mmol, 1.0 eq.). **13** was obtained as a white solid (5.70 g, 85%).

^{1}H NMR (400 MHz, $CDCl_3$) δ 9.20 (s, 1H), 7.93 (m, 1H), 7.76 (m, 1H), 7.35 (m, 2H), 3.62 (t, *J* = 6 Hz, 2H), 2.50 (t, *J* = 6.0 Hz, 2H), 2.10 (s, 6H). ^{13}C NMR (400 MHz, DMSO-*d*) δ 161.3, 147.4, 132.7, 129.3, 128.7, 126.7, 126.38, 59.8, 59.2. FTMS - c ESI $\{C_{11}H_{15}N_2O_3S\}^-$ [M-H] – calcd 255.0809, obsd 255.08113 (Δ=0.90).

15

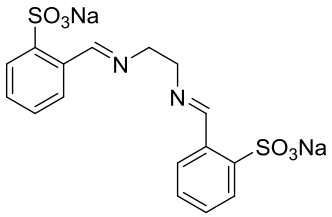

Synthesized from ethanol (24 mL), 2-formylbenzenesulfonic acid sodium salt (5.00 g, 24.06 mmol, 2.0 eq.), and ethylenediamine (0.803 mL, 0.723 g, 12.03 mmol, 1.0 eq.). **15** was obtained as a white solid (4.5 g, 85%).

^{1}H NMR (400 MHz, DMSO-*d*) δ 9.24 (s, 2H), 7.95 (dd, *J* = 8.0, 2.0 Hz, 2H), 7.74 (dd, *J* = 8.0, 2.0 Hz, 2H), 7.33 (m, 4H), 3.82 (s, 4H). ^{13}C NMR (400 MHz, DMSO-*d*) δ 161.9, 147.3, 132.7, 129.3, 128.8, 126.7, 61.6.

16

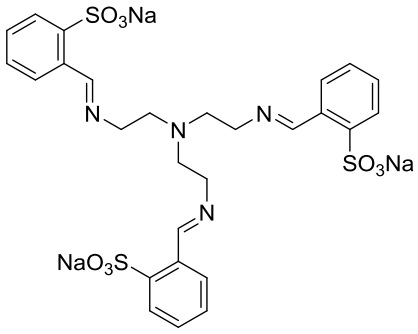

Synthesized from ethanol (20 mL), 2-formylbenzenesulfonic acid sodium salt (6.39 g, 30.69 mmol, 3.0 eq.), and tris(2-aminoethyl)amine (1.53 mL, 10.23 mmol, 1.0 eq.). **16** was obtained as a yellow solid (6.23 g, 85%).

^{1}H NMR (400 MHz, DMSO-*d*) δ 9.23(s, 3H), 7.95 (m, 3H), 7.75 (m, 3H), 7.35 (m, 6H), 3.69 (t, *J* = 6 Hz, 6H), 2.91 (t, *J* =6 Hz, 6H). ^{13}C NMR (400 MHz, DMSO-*d*) δ 161.3, 147.2, 132.8, 129.2, 128.8, 126.60, 126.55, 59.6, 55.2.

Preparation of Ligand 14

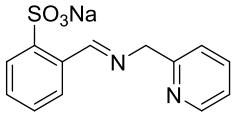

To a 100 mL round bottom, 2-formylbenzenesulfonic acid sodium salt (9.60 g, 46.02 mmol, 1.0 eq.) was added to methanol (20 mL, 2.3M) and Na_2SO_4 (6.53 g, 46.02

mmol, 1.0 eq.). To the reaction mixture, 2-picolylamine (4.76 mL, 46.02 mmol, 1 eq.) was added and stirred at room temperature for 8 hours. Upon completion, Na_2SO_4 was filtered out and the mixture was concentrated under reduced pressure to afford **14** as a white solid (11.0 g, 79%).

^{1}H NMR (300 MHz, DMSO-*d*) δ 9.39 (s, 1H), 8.52 (dd, *J* = 4.0, 0.9 Hz, 1H), 8.01 (m, 1H), 7.78 (m, 2H), 7.39 (m, 4H), 4.84 (s, 2H). ^{13}C NMR (400 MHz, DMSO-*d*) δ 162.9, 159.3, 148.9, 147.6, 136.8, 136.8, 132.5, 129.7, 128.9, 126.7, 126.5, 122.2, 66.3. FTMS - c ESI $\{C_{13}H_{11}N_2O_3S\}^-$ [M-H] – calcd 275.04959, obsd 275.04931 (Δ=1.02).

Ligand 16 Complexation Procedure

To a scintillation vial, MX_2 (1.0 eq., unless noted otherwise), **13** (2.0 eq.), and THF (0.16 M) were stirred at room temperature for 4 hours. The reaction mixture was concentrated under reduced pressure and the crude solids were redissolved in dichloromethane or acetonitrile. The crude solution was filtered through a short celite plug and concentrated under reduced pressure. The crude solids were redissolved into a minimum amount of dichloromethane or acetonitrile for crystallization through vapor diffusion or using a minimum amount of solvent.

Fe(**13**)$_2$

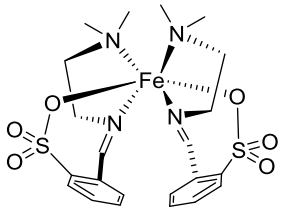

Synthesized from THF (32 mL), **13** (1.5 g, 5.38 mmol) and $FeCl_2$ (0.341 g, 2.19 mmol). The crude product was crystallized through vapor diffusion of pentane into concentrated dichloromethane solution to afford yellow crystals (1.10 g, 73%).

^{1}H NMR (400 MHz, $CDCl_3$) δ 104.72 (bs), 76.26 (bs), 66.24 (bs), 6.34 (bs), 5.19 (bs), 4.99 (bs), 3.33 (bs). IR (neat) cm^{-1} 3059, 3013, 2967, 2918, 2871, 2841, 2798, 1655, 1467, 1388, 1333, 1268, 1171, 1138, 1085, 1016, 949, 901, 782, 757, 734, 716, 622, 574, 545, 482.

[(**13**)$_2$Co$_2$(μ-Cl)$_2$]

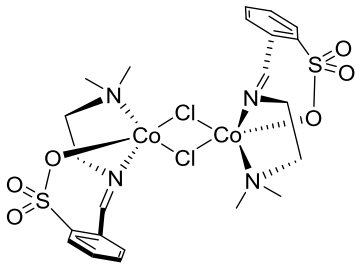

Synthesized from THF (10mL), **13** (250 mg, 1.60 mmol) and $CoCl_2$ (103 mg, 0.80 mmol, 2.0 eq.). The crude product was crystallized through vapor diffusion of pentane into concentrated dichloromethane solution to afford light purple crystals (251 mg, 40%).

^{1}H NMR (400 MHz, $CDCl_3$) δ 52.02 (bs), 47.53 (bs), 46.47 (bs), 24.94 (bs), 2.92 (bs), 2.77 (bs), 2.15(bs). IR (neat) cm^{-1} 3065, 3004, 2973, 2934, 2883, 2844, 2798, 1656, 1467, 1450, 1724, 1166, 1138, 1081, 1034, 1011, 990, 947, 770, 716, 624, 465.

Ni(**13**)$_2$

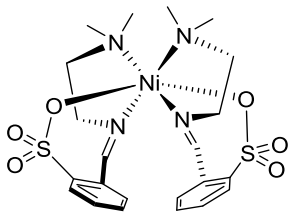

Synthesized from THF (10 mL), **13** (250 mg, 1.80 mmol) and $NiCl_2$ (116 mg, 0.90 mmol). The crude product was crystallized through a minimum amount of acetonitrile to afford teal crystalline plates (317 mg, 62%).

^{1}H NMR (400 MHz, $CDCl_3$) δ 11.00 (bs), 9.21 (bs), 7.88 (bs), 7.41 (bs), 3.76 (bs), 3.65 (bs), 2.43 (bs). IR (neat) cm^{-1} 3062, 3027, 2977, 2926, 2867, 1656, 1569, 1467, 1257, 1178, 1138, 1090, 1024, 948, 763, 717, 619, 573.

Mn(**13**)$_2$

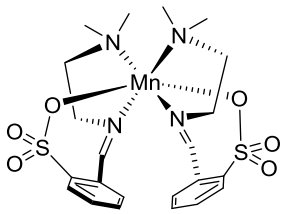

Synthesized from THF (10 mL), **13** (250 mg, 1.80 mmol), and $MnCl_2$ (113 mg, 0.90 mmol). The crude product was crystallized through vapor diffusion of pentane into concentrated dichloromethane solution to afford colorless crystals (330 mg, 65%).

^{1}H NMR (400 MHz, $CDCl_3$) δ 7.20 (bs), 3.75 (bs), 3.48 (bs), 2.02 (bs), 1.87 (bs), 0.89 (bs). IR (neat) cm^{-1} 3058, 2963, 2922, 2856, 2756, 1638, 1561, 1544, 1500, 1476, 1365, 1260, 1103, 1069, 955, 912, 794, 660, 662, 447, 412.

1. X-Ray Crystallography Data Collection and Refinement

In these studies, crystals were submitted for analysis in the solvents they were crystallized in. The crystal analysis was done by Dr. John Bacsa at Emory University. Polarized microscopy (between crossed polars) was used to select crystals that would diffract as single crystals and also to select better formed crystals.

In all cases, suitable crystals were selected from the sample and mounted quickly onto a nylon fibre with paratone oil and placed under a cold stream at 110(2) K. Single crystal X-ray data were collected on a Bruker APEX2 diffractometer with 1.6 kW graphite monochromated Mo radiation. The detector to the crystal distance was 5.1 cm. The data collection was performed using a combination of sets of ω scans yielding data in a reasonable 2θ range and average completeness. The frames were integrated with the SAINT v7.68a (Bruker, 2009).[59] For single crystals, multiscan absorption corrections were carried out using the program SADABS V2008-1 (Bruker, 2008).[60] For non-merohedrally twinned crystals multi-scan absorption corrections were carried out using the program TWINABS-2008/3 (Bruker, 2008).[60] Further details are given in the CIFs. The structures were solved with either SHELX (Sheldrick, 2008) or JANA2006 (Palatinus *et. al*, 2006)[61] and refined with Olex2 and SHELX (Sheldrick, 2008)[62].

	Fe(**13**)$_2$	Mn(**13**)$_2$	Ni(**13**)$_2$	[(**13**)$_2$Co$_2$(μ-Cl$_2$)]
Empirical Formula	$C_{24}H_{34}Cl_4FeN_4O_6S_2$	$C_{21}HN_4O_9SCl_5Mn$	$C_{24}H_{33}N_5NiO_6S_2$	$C_{22}H_{30}Cl_2Co_2N_4O_6S_2$
Formula weight	736.32	716.5	610.38	699.38
Temperature/K	110(2)	110(2)	110(2)	110(2)
Crystal system	monoclinic	monoclinic	monoclinic	monoclinic
Space group	C2/c	C2/c	$P2_1/c$	$P2_1$
a/Å	16.6030(10)	16.5608(4)	15.0831(19)	19.699(2)
b/Å	14.0521(9)	14.0621(3)	17.423(2)	6.8073(7)
c/Å	14.8172(9)	14.9814(3)	10.8060(14)	23.385(3)
a/°	90	90	90	90
b/°	108.2193(8)	108.6993(10)	105.8449(18)	114.7411(15)
g/°	90	90	90	90
volume/Å3	3283.6(4)	3304.70(13)	2731.8(6)	2848.0(5)
Z	4	4	4	4
Crystal size/mm3	0.636 x 0.360 x 0.184	0.441 x 0.238 x 0.218	0.390 x 0.276 x 0.185	0.531 x 0.146 x 0.126
F(000)	188	254	447	703
2Θ range for data collection	1.941 to 30.030	1.945 to 46.522	1.826 to 29.119	1.138 to 25.681
Reflections collected	18872	75274	29821	24930
Independent reflections	4807 [R(int) = 0.0297]	14729 [R(int) = 0.0272]	7329 [R(int) = 0.0569]	10558 [R(int) = 0.0367]
Data/restraints/parameters	4807/0/188	14729/55/254	7329/30/447	10558/337/703
Goodness-of-fit on F2	1.046	1.053	1.016	1.038
Final R indexes [I>=2σ (I)]	0.0401	0.0376	0.0436	0.0488
Final R indexes [all data]	R1 = 0.0457, wR2 = 0.1093	R1 = 0.0475, wR2 = 0.1045	R1 = 0.0727, wR2 = 0.1062	R1 = 0.0517, wR2 = 0.1198
Largest diff. peak/hole / e Å-3	0.83/-0.707	1.476/-0.958	0.528/-0.420	1.165/-0.617
CCDC code	n/a	n/a	n/a	n/a

2. O_2 Reactivity Experiments

The set up of the O_2 reactivity test requires the following items: 4 mL vial, small septum, and an O_2 balloon. The samples were prepared in the glovebox, and then the sample was purged with O_2 and prior to the O_2 balloon being appended. The O_2 reactivity test proceeded until the balloon deflated or changes were not able to be detected. Several solvents were tested with O_2 (Table S1).

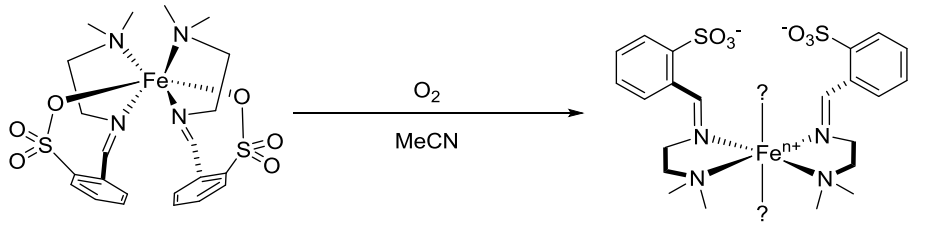

Solvent	Color(s)	Solvent left?	Solubility*
DCM	Orange w/ white solids	No	DMSO only
CCl4	Orange w/ white solids	No	DMSO only
MeCN	Orange solution	Yes	N/A
DMF	Orange solution	Yes	N/A
THF	Orange w/ white solids	No	DMSO only
*Solvents tried: DCM, THF, MeCN, PhMe			

Table S1. Solvents that are used and changed.

a. O_2 Uptake Experiment

The O2 uptake apparatus was assembled with the following glassware: Schlenk flask, Dean-Stark trap, long tip funnel, tygon tubing, O_2 balloon, and a septum. We dissolved 100 mg of the Fe(**13**)$_2$ complex in 10 mL of MeCN in a Schlenk flask in the glovebox. Then, we sealed off a Schlenk flask under N_2 and brought it out of the glove box. The Schlenk flask was then quickly connected to the Dean-Stark trap and one end of

the tygon tubing was fitted onto the long tipped funnel, while the other end was fitted onto the tip of the Dean-Stark trap. Once all assembled, an O_2 balloon was used to purge the system to ensure that it was under an O_2 atmosphere.

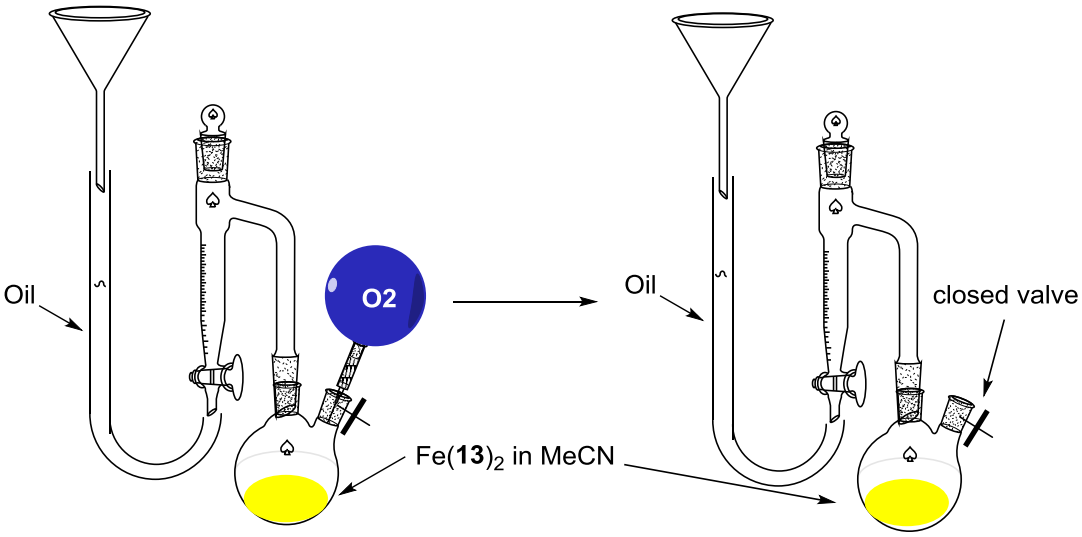

Figure S1. The assembled O_2 apparatus.

The system was purged again with an O_2 balloon as a precaution. Once the system was purged with O_2, the balloon was removed and the system was sealed off by closing the valve of the Schlenk flask. The volume of O_2 consumed was measured by the volume of mineral oil that entered the Dean-Stark trap. For the first O_2 uptake experiment, the data was recorded on an interval of 20 minutes for the first 3 hours. Afterwards the next time point was recorded after 12 hours and was checked on every hour thereafter (Figure S2).

A second O_2 uptake experiment was ran the same way except data points were obtained at 20 minute intervals over the course of 7 hours (Figure S3).

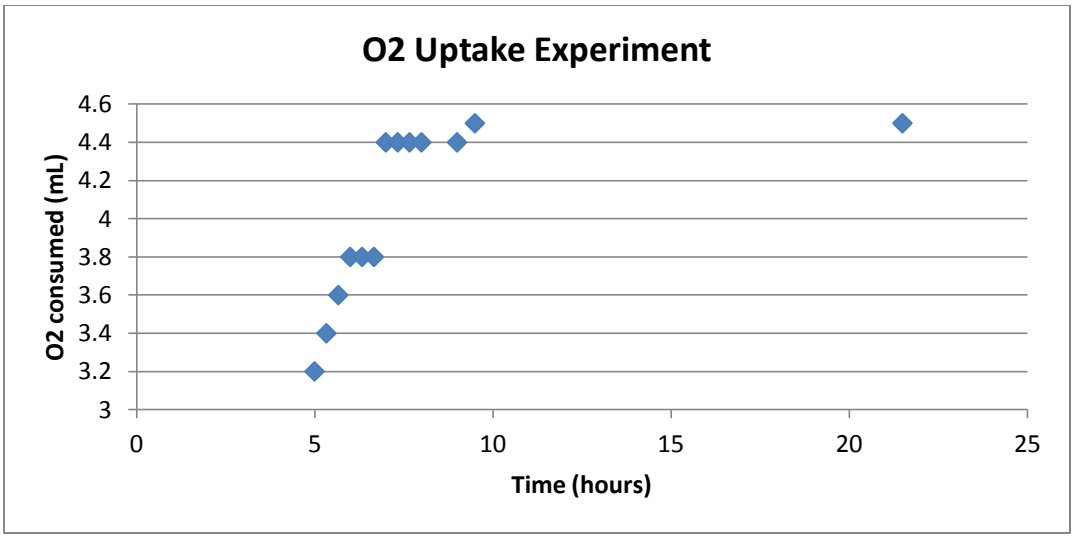

Figure S2. The O_2 uptake over the course of 24 hours with a 1.00:1.04 ratio of Fe:O_2.

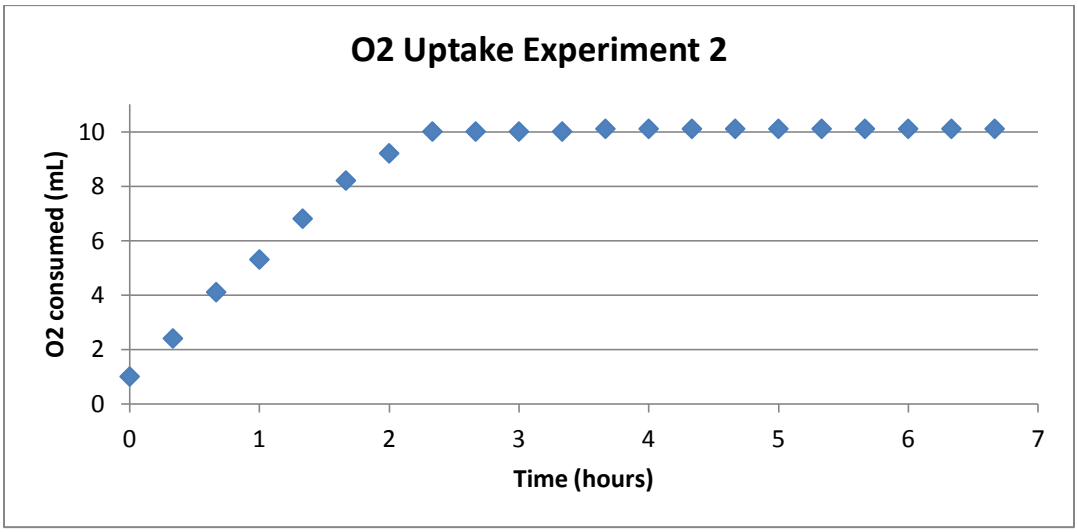

Figure S3. The second O_2 uptake experiment with Fe(**13**)$_2$ with a 2.01:1.00 ratio of Fe:O_2.

3. Cyclic Voltammetry

Cyclic voltammetry (CV) data for the complexes were conducted in acetonitrile with 0.1 M tetrabutyl ammonium hexafluorophosphate as the supporting electrolyte and platinum wire as the counter electrode. Non-aqueous $Ag^{+}/AgPF_6$ (0.01M) was used as a reference electrode and a glassy carbon electrode served as the working electrode. These data were recorded at a scan rate of 0.1 V/s. Reported electrochemical potentials have been referenced internally to the Fc/Fc^{+}.

Experimental Spectra

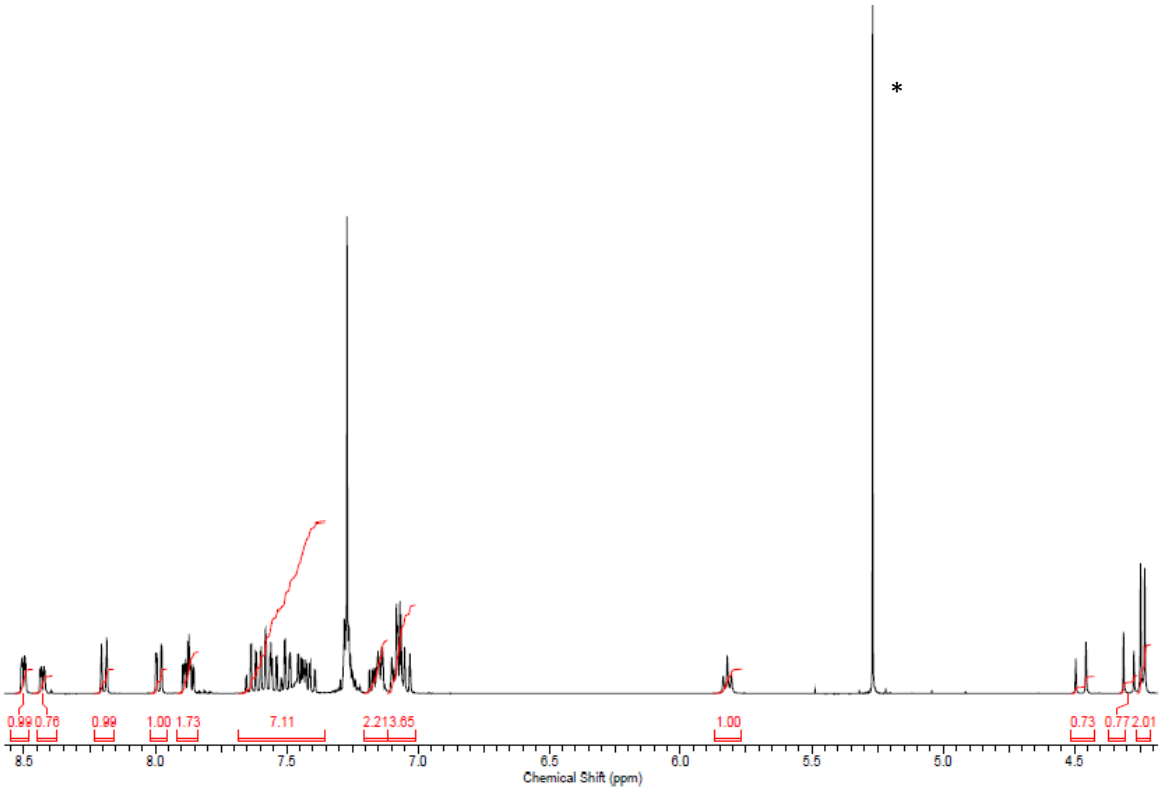

Figure S4. ^{1}H NMR spectrum of **10**. *Solvent peak for dichloromethane.

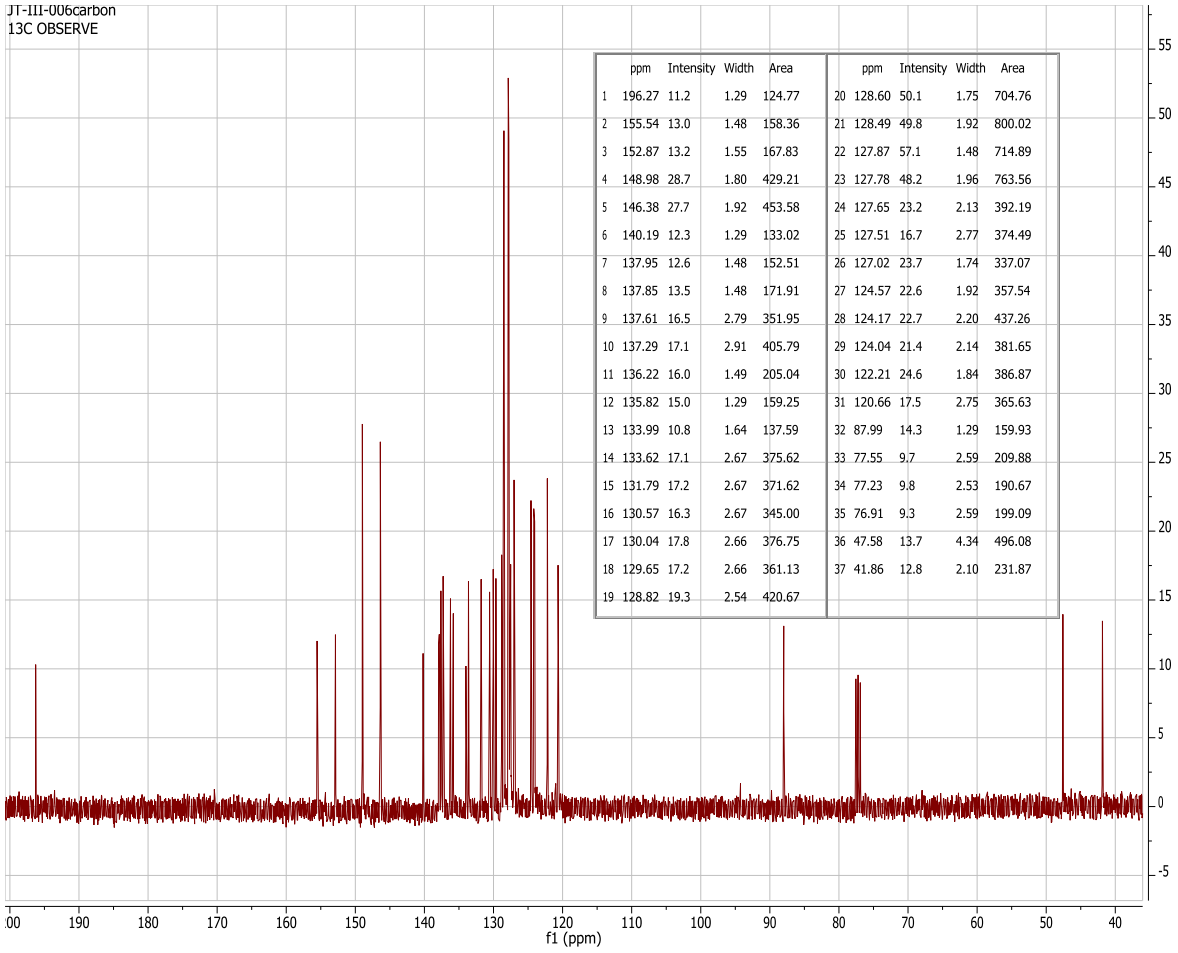

	ppm	Intensity	Width	Area		ppm	Intensity	Width	Area
1	196.27	11.2	1.29	124.77	20	128.60	50.1	1.75	704.76
2	155.54	13.0	1.48	158.36	21	128.49	49.8	1.92	800.02
3	152.87	13.2	1.55	167.83	22	127.87	57.1	1.48	714.89
4	148.98	28.7	1.80	429.21	23	127.78	48.2	1.96	763.56
5	146.38	27.7	1.92	453.58	24	127.65	23.2	2.13	392.19
6	140.19	12.3	1.29	133.02	25	127.51	16.7	2.77	374.49
7	137.95	12.6	1.48	152.51	26	127.02	23.7	1.74	337.07
8	137.85	13.5	1.48	171.91	27	124.57	22.6	1.92	357.54
9	137.61	16.5	2.79	351.95	28	124.17	22.7	2.20	437.26
10	137.29	17.1	2.91	405.79	29	124.04	21.4	2.14	381.65
11	136.22	16.0	1.49	205.04	30	122.21	24.6	1.84	386.87
12	135.82	15.0	1.29	159.25	31	120.66	17.5	2.75	365.63
13	133.99	10.8	1.64	137.59	32	87.99	14.3	1.29	159.93
14	133.62	17.1	2.67	375.62	33	77.55	9.7	2.59	209.88
15	131.79	17.2	2.67	371.62	34	77.23	9.8	2.53	190.67
16	130.57	16.3	2.67	345.00	35	76.91	9.3	2.59	199.09
17	130.04	17.8	2.66	376.75	36	47.58	13.7	4.34	496.08
18	129.65	17.2	2.66	361.13	37	41.86	12.8	2.10	231.87
19	128.82	19.3	2.54	420.67					

Figure S5. 30 Carbons are shown here in the ^{13}C Spectrum of **10**. Key peaks are 196.3 ppm and 87.9 ppm.

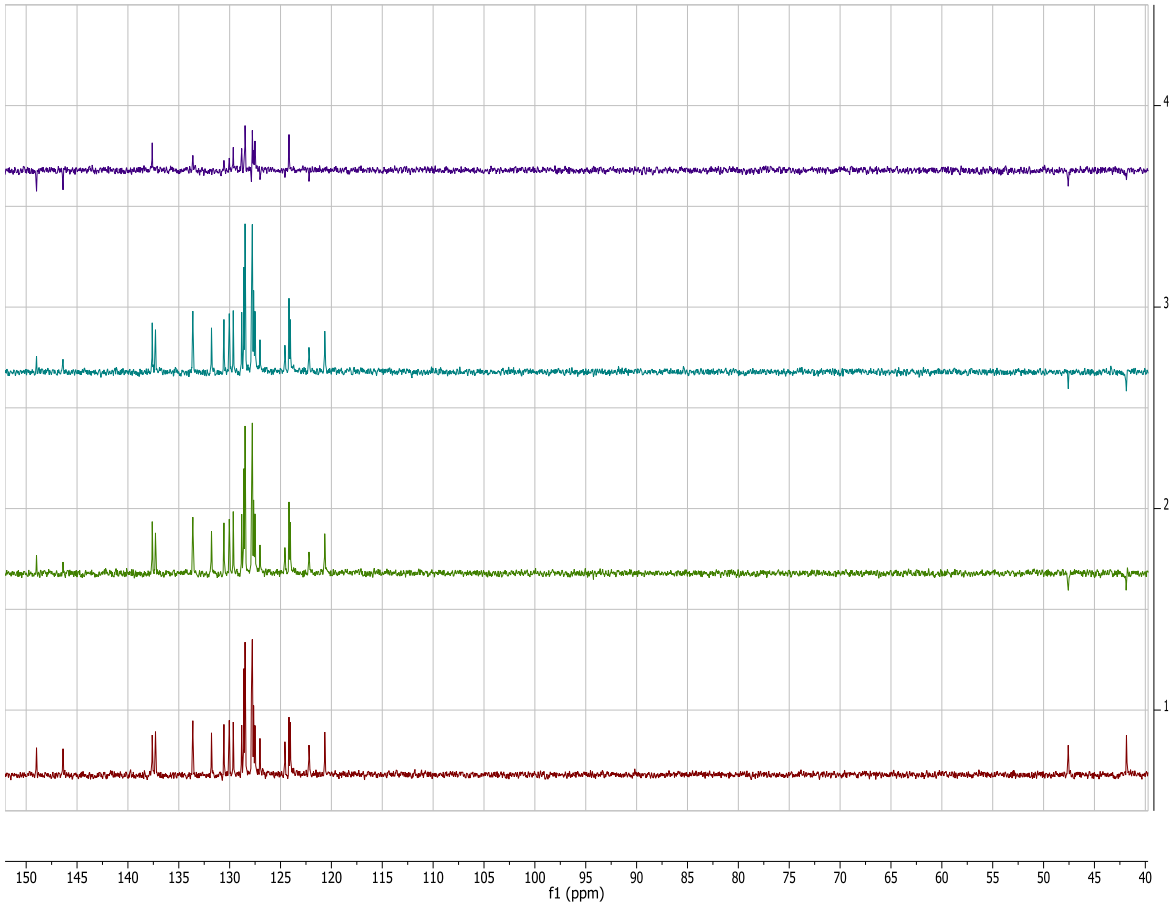

Figure S6. DEPT spectra of **10** is shown here where absent peaks at 196.3 ppm and 87.9 ppm are the ketone and alcohol quaternary carbons.

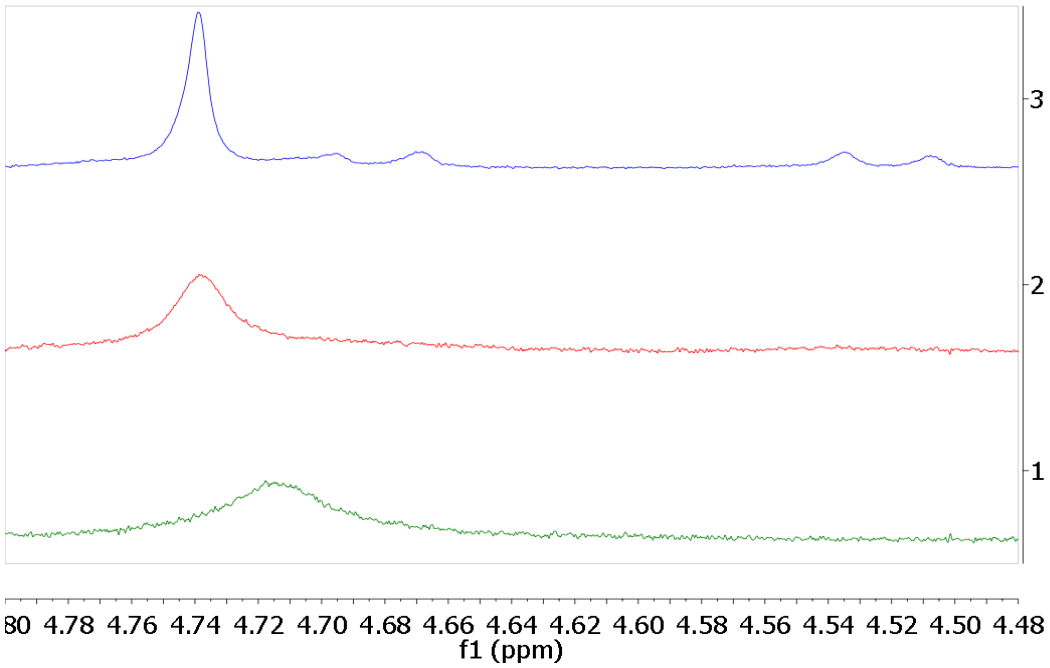

Figure S7. VT NMR spectra of compound **12d** focused on the benzylic protons taken at room temperature (spectrum 3), 50 ºC (spectrum 2), and 80 ºC (spectrum 1).

6.0 Appendix

6.1 Synthesis of $Fe(14)_2/Fe(14)_3X$

One of the promising ligands generated in this study was **14**. However, there were many difficulties in metallating **14** onto the Fe^{II} center. The problem that arose from the metallation of **14** onto Fe^{II} was that a large amount of insoluble solids would crash out regardless of the equivalents of **14** (Scheme A1).

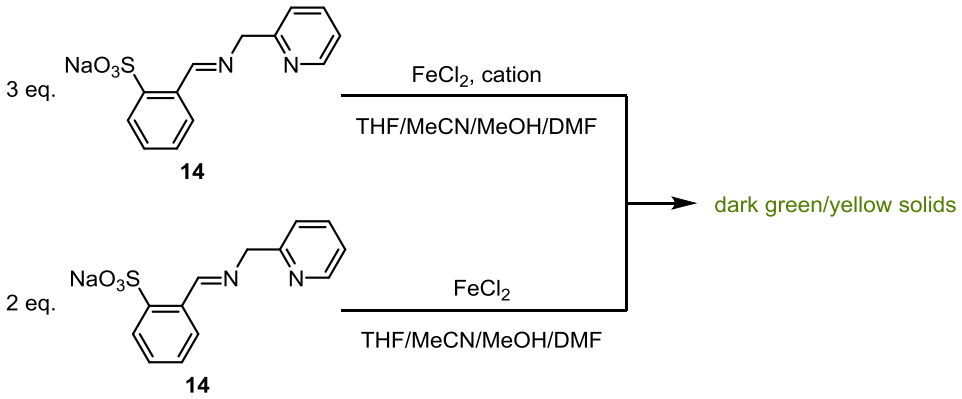

Scheme A1. Metallation of **14** to $FeCl_2$ salt produces insoluble dark green solids.

Only small amounts of the dark green/yellow solids were soluble in DMF, while other solvents only provided minimum solubility. Attempts at crystallizations of soluble dark green/yellow solids of the 3 equivalents of **14** metallation yielded only tetraethylammonium bromide. When the metallation of **14** was attempted in different solvents, all the mixtures eventually converged on a dark green/yellow solution after one hour. However, the initial color changes were similar in different solvents before the one hour mark, suggesting the metallation may have finished earlier (Table A1).

Table A1. Initial color changes of metallation of **14** to $FeCl_2$ in three different solvents.

Solvent	**Color(s) Observed**
MeCN	Yellow/Orange
DMF	Maroon
MeOH	Orange/red

A potential solution could be to exchange the sodium of **14** with an organic cation, such as ammoniums or phosphoniums. There is a possibility that the imino-pyridine platform could be chelating to the sodium, reducing the amount of ligands that could actually bind to the Fe^{II} metal center. By exchanging the cation, compound **14** could become more soluble in organic solvents that are available in the glovebox.

6.2 Synthesis of M(16)

Another promising ligand that was generated in this study was ligand **16**. Ligand **16** is an attractive ligand as it enforces a trigonal bipyramidal geometry leaving one coordination site open for potential atom/group transfer reactivity (Scheme A2).

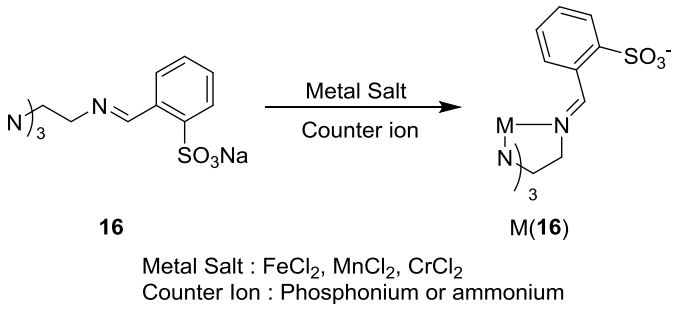

Scheme A2. Metallation of **16** to different metal salts.

There were many difficulties, however, in generating the desired metal complexes with **16**. Crystallization attempts of the Fe^{II}, Mn^{II}, and Cr^{II} complexes with different cations like tetrabutylammonium, tetraethylammonium, and tetraphenylphosphonium only resulted in tetrahalogenated metal salts. Initial metallations utilized tetrabutylammonium cation for crystallization attempts; however, nothing was crystallized after varying the solvents, which could be due to the butyl groups. As a result, tetraethylammonium and tetraphenylphosphonium were used due to the success observed in our lab with those cations in crystallizations. Initially, crystalline material of

what could have been the [Mn(**16**)PPh_4] were observed. Unfortunately, it was later found that the crystals were actually $[Mn(Cl)_4](PPh_4)_2$.

A potential solution to this problem could be to change the metal salts, considering chlorides have been observed to stay bound to the first row transition metals like manganese, iron, and cobalt. It is possible that metal triflate salts may have success in forming the M(**16**) complex since triflates are weakly coordinating anions compared to halogens.

6.3 O_2 Reactivity with Fe(13)$_2$

When the Fe(**13**)$_2$ complex was isolated and fully characterized, O_2 studies were conducted on the complex due to the suggestive data from the CV. Fe(**13**)$_2$ CV showed different redox potentials when placed in acetonitrile compared to dichloromethane, potentially due to acetonitrile displacing the sulfonates and allowing for the conversion of the imine to the amido chelate. From the CV result, O_2 reactivity studies were performed, but revealed inconsistent results. In the initial attempt, there was a ratio of 1.04:1.00 of O_2 to the Fe(**13**)$_2$ complex (Figure S2). These initial attempt's resulted revealed the potential of a peroxo-like species with the Fe(**13**)$_2$ complex. However a second O_2 uptake experiment resulted in a 2.01:1.00 of O_2 to the Fe(**13**)$_2$ complex (Figure S3).

The inconsistent results from the O_2 uptake experiments, especially the second time, proved to be problematic as it suggests a di-peroxo iron species. Furthermore, crystallization attempts of the mixture to identify the products of the O_2 reactivity studies revealed a zwitterionic ligand from the crude mixture. The experiment should be repeated to identify other products that are in the mixture and ideally address what happened to the iron. Initial predictions were that once the complex was exposed to O_2, it decomposed

into the polymeric Fe_2O_3. However, there were no indications of Fe_2O_3. In order to resolve these inconsistent results, a better O_2 apparatus must be constructed, as the current apparatus does expose Fe(**13**)$_2$ to the atmosphere in the process of assembling the O_2 uptake apparatus.

6.4 Revisiting the Synthesis of 12d

In the synthesis **12d**, the major setbacks were the pyridyl addition to form the keto-pyridine and subsequent amine condensation to generate the desired imino-pyridine where yields were 20% and 30%, respectively.

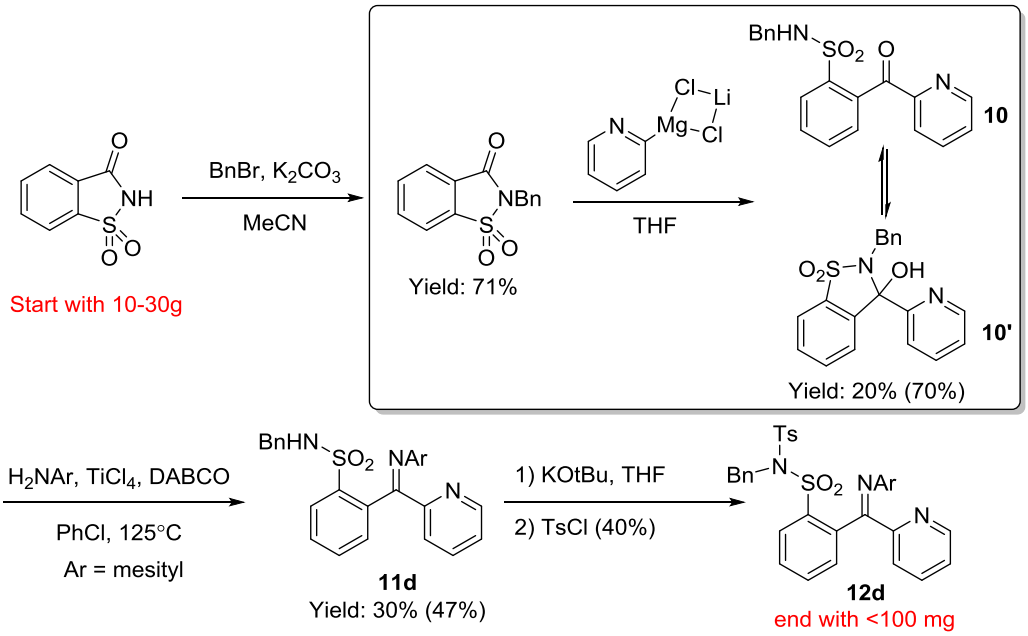

Scheme A3. Rational synthesis of ERLs with the focus on optimizing the pyridyl turbo Grignard addition to the benzyl saccharin.

Several conditions were explored in order to optimize these steps, specifically the pyridyl addition to benzyl saccharin. We also attempted using different organometallic reagents, such as organocerium, organolithium, organozinc, Grignard, and the turbo Grignard, but none of these reagents improved the yield.[50,51,63,64] In addition, there were

attempts to use chelating reagents, such as tetramethylethylenediamine and 1,4-dioxane, to increase the nucleophilicity of the organometallic pyridine, but again the yields did not change.

A potential solution to the low yields for the pyridyl addition could be the addition of a Lewis acid that could activate the amide of the benzyl saccharin. Lewis acids that should be tried in this case are aluminum trichloride and a boron trifluoride tetrahydrofuran complex.[65]

7.0 References

(1) Leeuwen, P. W. N. M. van. *Homogeneous Catalysis: Understanding the Art*; 2004th ed.; Springer, 2004.

(2) Keith, J. A.; Henry, P. M. *Angew. Chem. Int. Ed.* **2009**, *48*, 9038–9049.

(3) Jira, R. *Angew. Chem. Int. Ed.* **2009**, *48*, 9034–9037.

(4) Nobelprize.org http://www.nobelprize.org/nobel_prizes/chemistry/laureates/ (accessed Apr 12, 2013).

(5) Louis Hegedus; Soderberg, B. *Transition Metals in the Synthesis of Complex Organic Molecules*; 3rd ed.; University Science Books, 2009.

(6) Punniyamurthy, T.; Velusamy, S.; Iqbal, J. *Chem. Rev.* **2005**, *105*, 2329–2364.

(7) Gopalaiah, K. *Chem. Rev.* **2013**, *113*, 3248–3296.

(8) Cahiez, G.; Moyeux, A. *Chem. Rev.* **2010**, *110*, 1435–1462.

(9) Rosen, B. M.; Quasdorf, K. W.; Wilson, D. A.; Zhang, N.; Resmerita, A.-M.; Garg, N. K.; Percec, V. *Chem. Rev.* **2011**, *111*, 1346–1416.

(10) Sheldon, R. A.; Arends, I. W. C. E.; ten Brink, G.-J.; Dijksman, A. *Acc. Chem. Res.* **2002**, *35*, 774–781.

(11) Zhan, B.-Z.; Thompson, A. *Tetrahedron* **2004**, *60*, 2917–2935.

(12) Mallat, T.; Baiker, A. *Chem. Rev.* **2004**, *104*, 3037–3058.

(13) Markó, I. E.; Giles, P. R.; Tsukazaki, M.; Chellé-Regnaut, I.; Gautier, A.; Dumeunier, R.; Philippart, F.; Doda, K.; Mutonkole, J.-L.; Brown, S. M.; Urch, C. J. In *Advances in Inorganic Chemistry*; R. van Eldik, Ed.; Academic Press, 2004; Vol. Volume 56, pp. 211–240.

(14) Schultz, M. J.; Sigman, M. S. *Tetrahedron* **2006**, *62*, 8227–8241.

(15) In *Catalysis without Precious Metals*; Bullock, R. M., Ed.; Wiley-VCH Verlag GmbH & Co. KGaA, 2010; pp. 277–290.

(16) Johnson, D. A.; Nelson, P. G. *Inorg. Chem.* **1999**, *38*, 4949–4955.

(17) Daul, C.; Goursot, A. *Inorg. Chem.* **1985**, *24*, 3554–3558.

(18) Figgis, B. N.; Hitchman, M. *Ligand Field Theory and Its Applications*; Wiley-VCH: New York, 2000.

(19) Archer, A. M.; Bouwkamp, M. W.; Cortez, M.-P.; Lobkovsky, E.; Chirik, P. J. *Organometallics* **2006**, *25*, 4269–4278.

(20) Lyaskovskyy, V.; de Bruin, B. *ACS Catal.* **2012**, *2*, 270–279.

(21) Chirik, P. J.; Wieghardt, K. *Science* **2010**, *327*, 794–795.

(22) Luca, O. R.; Crabtree, R. H. *Chem. Soc. Rev.* **2013**, *42*, 1440–1459.

(23) Darmon, J. M.; Stieber, S. C. E.; Sylvester, K. T.; Fernández, I.; Lobkovsky, E.; Semproni, S. P.; Bill, E.; Wieghardt, K.; DeBeer, S.; Chirik, P. J. *J. Am. Chem. Soc.* **2012**, *134*, 17125–17137.

(24) Hojilla Atienza, C. C.; Tondreau, A. M.; Weller, K. J.; Lewis, K. M.; Cruse, R. W.; Nye, S. A.; Boyer, J. L.; Delis, J. G. P.; Chirik, P. J. *ACS Catal.* **2012**, *2*, 2169–2172.

(25) Monfette, S.; Turner, Z. R.; Semproni, S. P.; Chirik, P. J. *J. Am. Chem. Soc.* **2012**, *134*, 4561–4564.

(26) Tondreau, A. M.; Lobkovsky, E.; Chirik, P. J. *Org. Lett.* **2008**, *10*, 2789–2792.

(27) Trovitch, R. J.; Lobkovsky, E.; Bouwkamp, M. W.; Chirik, P. J. *Organometallics* **2008**, *27*, 6264–6278.

(28) Yu, R. P.; Darmon, J. M.; Hoyt, J. M.; Margulieux, G. W.; Turner, Z. R.; Chirik, P. J. *ACS Catal.* **2012**, *2*, 1760–1764.

(29) Lippard, S. J.; Gray, H. B.; Bertini, I. *Bioinorganic Chemistry*; University Science Books: Mill Valley, CA, 1994.

(30) Pellissier, H.; Clavier, H. *Chem. Rev.* **2014**, *114*, 2775–2823.

(31) Rodgers, G. E. *Descriptive Inorganic, Coordination, and Solid-State Chemistry*; 2nd ed.; Thomson Learning, 2002.

(32) Amatore, C.; Jutand, A. *Acc. Chem. Res.* **2000**, *33*, 314–321.

(33) McDonald, A. R.; Que Jr., L. *Coord. Chem. Rev.* **2013**, *257*, 414–428.

(34) Collins, T. J.; Gordon-Wylie, S. W. *J. Am. Chem. Soc.* **1989**, *111*, 4511–4513.

(35) Pfaff, F. F.; Kundu, S.; Risch, M.; Pandian, S.; Heims, F.; Pryjomska-Ray, I.; Haack, P.; Metzinger, R.; Bill, E.; Dau, H.; Comba, P.; Ray, K. *Angew. Chem. Int. Ed.* **2011**, *50*, 1711–1715.

(36) Berry, J. F. *Comments on Inorganic Chemistry* **2009**, *30*, 28–66.

(37) Kitchen, J. A.; Noble, A.; Brandt, C. D.; Moubaraki, B.; Murray, K. S.; Brooker, S. *Inorg. Chem.* **2008**, *47*, 9450–9458.

(38) De Visser, S. P.; Rohde, J.-U.; Lee, Y.-M.; Cho, J.; Nam, W. *Coord. Chem. Rev.* **2013**, *257*, 381–393.

(39) Berry, J. F. *Comments on Inorganic Chemistry* **2009**, *30*, 28–66.

(40) Bordwell, F. G.; Algrim, D. *J. Org. Chem.* **1976**, *41*, 2507–2508.

(41) Chataigner, I.; Panel, C.; Gérard, H.; Piettre, S. R. *Chem. Commun.* **2007**, 3288–3290.

(42) Hansch, C.; Leo, A.; Taft, R. W. *Chem. Rev.* **1991**, *91*, 165–195.

(43) Valters, R. E.; Füöp, F.; Korbonits, D. In *Advances in Heterocyclic Chemistry*; Alan R. Katritzky, Ed.; Academic Press, 1995; Vol. Volume 64, pp. 251–321.

(44) Jones, P. R. *Chem. Rev.* **1963**, *63*, 461–487.

(45) Antoniotti, S.; Dalla, V.; Duñach, E. *Angew. Chem. Int. Ed.* **2010**, *49*, 7860–7888.

(46) Bordwell, F. G. *Acc. Chem. Res.* **1988**, *21*, 456–463.

(47) DeChristopher, P. J.; Adamek, J. P.; Lyon, G. D.; Klein, S. A.; Baumgarten, R. J. *J. Org. Chem.* **1974**, *39*, 3525–3532.

(48) Figuly, G. D.; Martin, J. C. *J. Org. Chem.* **1980**, *45*, 3728–3729.

(49) Bonfiglio, J. N. *J. Org. Chem.* **1986**, *51*, 2833–2835.

(50) Paquette, L. A.; Dura, R. D.; Modolo, I. *J. Org. Chem.* **2009**, *74*, 1982–1987.

(51) Krasovskiy, A.; Knochel, P. *Angew. Chem. Int. Ed.* **2004**, *43*, 3333–3336.

(52) Cogan, D. A.; Ellman, J. A. *J. Am. Chem. Soc.* **1999**, *121*, 268–269.

(53) Suzuki, M.; Nakajima, R.; Tsuruta, M.; Higuchi, M.; Einaga, Y.; Yamamoto, K. *Macromolecules* **2006**, *39*, 64–69.

(54) Koppel, I. A.; Taft, R. W.; Anvia, F.; Zhu, S.-Z.; Hu, L.-Q.; Sung, K.-S.; DesMarteau, D. D.; Yagupolskii, L. M.; Yagupolskii, Y. L. *J. Am. Chem. Soc.* **1994**, *116*, 3047–3057.

(55) Demadis, K. D.; Hartshorn, C. M.; Meyer, T. J. *Chem. Rev.* **2001**, *101*, 2655–2686.

(56) Shejwalkar, P.; Rath, N. P.; Bauer, E. B. *Dalton Trans.* **2011**, *40*, 7617–7631.

(57) Fujita, T.; Lehn, J.-M. *Tetrahedron Lett.* **1988**, *29*, 1709–1712.

(58) Ferreira, L. C.; Filgueiras, C. A. L.; Visentin, L. C.; Bordinhaõ, J.; Hörner, M. *Z. Anorg. Allg. Chem.* **2009**, *635*, 1225–1230.

(59) *SAINT, V7.68A*; Bruker AXS Inc.: Madison, WI USA, 2009.

(60) *SADABS, V2008-1*; Bruker AXS Inc.: Madison, WI USA, 2008.

(61) Petricek, V.; Dusek, M.; Palatinus, L. *Jana6: The crystallographic computing system*; Institute of Physics: Praha, Czech Republic, 2006.

(62) Sheldrick, G. M. *Acta Crystallographica Section A Foundations of Crystallography* **2008**, *64*, 112–122.

(63) García, F.; Hopkins, A. D.; Kowenicki, R. A.; McPartlin, M.; Rogers, M. C.; Silvia, J. S.; Wright, D. S. *Organometallics* **2006**, *25*, 2561–2568.

(64) Johnson, C. R.; Tait, B. D. *J. Org. Chem.* **1987**, *52*, 281–283.

(65) Yamazaki, N.; Suzuki, H.; Kibayashi, C. *J. Org. Chem.* **1997**, *62*, 8280–8281.